THE ASTROPHYSICAL JOURNAL, 326:1–18, 1988 March 1


# GALACTIC EVOLUTION AND COSMOLOGY: PROBING THE COSMOLOGICAL DECELERATION PARAMETER

YUZURU YOSHII[1]
Tokyo Astronomical Observatory, University of Tokyo

AND

FUMIO TAKAHARA[2]
Nobeyama Radio Observatory, Tokyo Astronomical Observatory, University of Tokyo
*Received 1987 January 29; accepted 1987 August 14*

## ABSTRACT

The magnitude-redshift relation, the color-redshift relation, the galaxy number count, the redshift distribution of galaxies, and the extragalactic background light are calculated taking into account the effect of galactic evolution for several values of the cosmological deceleration parameter $q_0$ and the redshift of galaxy formation $z_F$. The spectral evolutions of galaxies for five morphological types E/S0, Sab, Sbc, Scd, and Sdm are simulated on the basis of the models of Arimoto and Yoshii. According to recent observations of faint elliptical galaxies, the magnitude-redshift relation favors high $q_0$ models, whereas the galaxy number count favors low $q_0$ models. It is found that, without the effect of galactic evolution, these two observations cannot be reproduced simultaneously by a single value of $q_0$. We show that this apparent inconsistency vanishes if the evolutionary brightening of early-type galaxies in the past is taken into account. All the existing data are compatible with the deceleration parameter $q_0 \sim 0.5$ provided that galaxies are formed at redshift $z_F \sim 3$–5. The predicted near-IR background light is an order of magnitude lower in the energy flux than the recent observations by Matsumoto, Akiba, and Murakami so that it may be attributed to other origins.

*Subject headings:* cosmology — galaxies: evolution — galaxies: photometry

## I. INTRODUCTION

Observations of faint galaxies are closely related to galactic evolution and cosmology. After Sandage (1961) proposed various observational tests which are able to determine the cosmological model, much effort has been made to obtain data in the regime of magnitude and redshift where such tests are sensitive to the cosmological deceleration parameter $q_0$, the redshift of galaxy formation $z_F$, and the past luminosities of galaxies (see the reviews by Ellis 1983 and Spinrad 1986). In near future the Hubble Space Telescope and other facilities including CCD camera will provide further information on galaxies at faint limiting magnitudes in optical and infrared passbands. Particularly, there is a great merit of using infrared passbands where uncertain ultraviolet spectrum of galaxies hardly affects the cosmological studies up to fairly large redshift.

In spite of accumulation of modern data, we face a problem that luminosity evolution of galaxies has large influence upon interpretation of observational results. Early attempt of simulating galactic evolution was made by Tinsley and her collaborators (Tinsley 1968, 1972; Larson and Tinsley 1974; Tinsley and Gunn 1976). Since their evolution models were too coarse to give firm constraint on $q_0$ and $z_F$, Tinsley (1977) confined herself to suggesting which observational test is more sensitive to each of the parameters.

Theoretical investigation on galactic evolution has made steady progress, and recent elaborate models are able to reproduce most properties of present-day galaxies. Bruzual and Kron (1980) and Bruzual (1983*a*) computed the evolving energy spectra of galaxies of various Hubble types from ultraviolet to infrared regions ($\lambda \sim 0.1$–$2$ $\mu$m). More recently, Arimoto and Yoshii (1986, 1987) developed a program of evolutionary population synthesis consistent with chemical evolution of galaxies and computed the evolving energy spectra of galaxies from optical to infrared regions ($\lambda \sim 0.4$–$3$ $\mu$m). It is hoped that these evolution models serve for more sensitive determination of the cosmological model.

Previous authors who intended to constrain the cosmological model focused attention on either of the magnitude-redshift relation (e.g., Lilly and Longair 1984; Lebofsky and Eisenhardt 1986; Djorgovski and Spinrad 1987) or the galaxy number count (e.g., Bruzual and Kron 1980; Tinsley 1980; Shanks *et al.* 1984; King and Ellis 1985), but it is unfortunate that the evolution models of galaxies they used are not always the same and that the scatter in observational data lowers the feasibility of each test. However, if a single set of the evolution models are used, incorporation of various tests still proves effective because the tests are differently dependent on $q_0$ and $z_F$. For this reason, in this paper, using Arimoto and Yoshii (1986, 1987) models of galactic evolution, we examine most of the proposed tests simultaneously and narrow an allowable range of such parameters. We also present many predictions which provide a guide to future observations. Section II describes the empirical properties of nearby galaxies and the theoretical framework of modeling faint and high-redshift galaxies. Sections III–V are devoted to the magnitude-redshift relation for giant elliptical galaxies, the galaxy number count, and the extragalactic background light, respectively. In all these sections the theoretical predictions are compared with recent observations as far as possible. In § VI we summarize our results.

[1] Also at Mount Stromlo and Siding Spring Observatories.
[2] Present affiliation, Tokyo Astronomical Observatory, University of Tokyo.

## II. MODEL CONSTRUCTION

### a) Cosmological Parameters

Let $f_\lambda(z)d\lambda$ be the spectral luminosity between $\lambda$ and $\lambda + d\lambda$ emitted from a galaxy at redshift $z$. Then the energy flux $S_\lambda$ between $\lambda$ and $\lambda + d\lambda$ received by an observer is given by (see Weinberg 1972)

$$S_\lambda\, d\lambda = \frac{1}{4\pi\, d_L^2} f_{\lambda/(1+z)}(z)\, \frac{d\lambda}{1+z}\,, \tag{1}$$

where $d_L$ is the luminosity distance. This relation is expressed as a relation between magnitude and distance:

$$m_\lambda = M_\lambda + K_\lambda(z) + E_\lambda(z) + 5\,\log\,(d_L/10\ \mathrm{pc})\,, \tag{2}$$

with

$$K_\lambda(z) = -2.5\,\log\,\frac{\int_0^\infty f_{\lambda'/(1+z)}(0)R_\lambda(\lambda')d\lambda'/(1+z)}{\int_0^\infty f_{\lambda'}(0)R_\lambda(\lambda')d\lambda'}\,, \tag{3}$$

and

$$E_\lambda(z) = -2.5\,\log\,\frac{\int_0^\infty f_{\lambda'/(1+z)}(z)R_\lambda(\lambda')d\lambda'}{\int_0^\infty f_{\lambda'/(1+z)}(0)R_\lambda(\lambda')d\lambda'}\,, \tag{4}$$

where $R_\lambda(\lambda')$ is the sensitivity function around an effective wavelength $\lambda$, and $K_\lambda(z)$ and $E_\lambda(z)$ are the correction factors for the frequency shift due to change in redshft and the luminosity evolution of a galaxy, respectively.

In the Friedmann model with zero cosmological constant, the luminosity distance $d_L$ is defined as

$$d_L = \frac{c}{H_0\, q_0^2}\,\{q_0\, z + (q_0 - 1)[(1 + 2q_0\, z)^{1/2} - 1]\}\,, \tag{5}$$

where $H_0$, $q_0$, and $c$ are the Hubble constant, the deceleration parameter, and the light velocity, respectively. For use in the following sections, the comoving volume $V(z)$ and the cosmological time $t(z)$ differentiated with respect to $z$ are given by

$$\frac{dV}{dz} = \frac{4\pi c\, d_L^2}{H_0(1+z)^3(1+2q_0\, z)^{1/2}}\,, \tag{6}$$

and

$$\frac{dt}{dz} = -\frac{1}{H_0(1+z)^2(1+2q_0\, z)^{1/2}}\,, \tag{7}$$

respectively. The age $t_G(z)$ of a galaxy formed at redshift $z_F$ is given by

$$t_G(z) = t(z) - t(z_F)\,. \tag{8}$$

To be consistent with the age $\sim$15 Gyr of Galactic globular clusters (e.g., Demarque and McClure 1977), we restrict ourselves to $H_0 = 50$ km s$^{-1}$ Mpc$^{-1}$. All the subsequent results without luminosity evolution of galaxies are independent of this parameter. In the other case, with evolution, the effect of larger $H_0$ is similar to the effect of larger $q_0$ or smaller $z_F$ through the age-redshift relation in equation (8).

### b) Local Properties of Present-Day Galaxies

We classify galaxies into five morphological types of E/S0, Sab, Sbc, Scd, and Sdm. (We make no distinction between $E$ and S0 galaxies). Various authors have obtained the relative proportions of these types brighter than $B_J = 16.5$ mag in the general field, and the local galaxy mix has been determined so as to reproduce the observed proportions at $B_J = 16.5$ mag. Pence (1976), Tinsley (1980), and Ellis (1983) derived the galaxy mix based on the different data sources of the Bright Galaxy Catalog (de Vaucouleurs 1963), the KOS Redshift Survey (Kirschner, Oemler, and Schechter 1978), and the Durham/AAT Redshift Survey (DARS), respectively. Their mixes are tabulated in Table 1. Throughout this paper we adopt the Tinsley mix. The proportion of E/S0 in the Tinsley mix is similar to the others, but the Tinsley mix is less abundant in Scdm, as confirmed by recent observations (e.g., the review by Ellis 1983). Since early-type galaxies become dominant in number at faint magnitudes (Tinsley 1977), our choice of the Tinsley mix does not change the conclusion significantly.

TABLE 1

RELATIVE PROPORTIONS OF GALAXY TYPES

| E/S0 | Sab | Sbc | Scd | Sdm | References |
|---|---|---|---|---|---|
| 0.215 | 0.185 | 0.160 | 0.275 | 0.165 | P |
| 0.321 | 0.281 | 0.291 | 0.045 | 0.061 | T(adopted) |
| 0.28 | 0.47 | | 0.25 | | E |

REFERENCES.—P, Pence 1976; T, Tinsley 1980; E, Ellis 1983.

The luminosity function of galaxies is assumed to have a Schechter form (Schechter 1976):

$$\varphi(L)dL = \varphi^*(L/L^*)^\alpha\,\exp\,(-L/L^*)d(L/L^*)\,, \tag{9a}$$

or equivalently

$$\psi(M)dM = 0.92\varphi^*\,\exp\,\{-0.92(\alpha+1)(M-M^*) - \exp\,[-0.92(M-M^*)]\}dM\,, \tag{9b}$$

where $\alpha$ is a constant index, $\varphi^*$ is a constant coefficient which has a dimension of the number density of galaxies, $L^*$ is the characteristic luminosity, and $M^*$ is the characteristic magnitude. Then the local densitiies of number and luminosity are given by

$$n_0 = \varphi^*_{50}(H_0/50)^3\Gamma(1+\alpha,\,\beta)\,, \tag{10}$$

and

$$\mathscr{L}_0 = L^*_{50}\,\varphi^*_{50}(H_0/50)\Gamma(2+\alpha,\,\beta)\,, \tag{11}$$

respectively, where $\Gamma(1+\alpha,\,\beta)$ and $\Gamma(2+\alpha,\,\beta)$ are the incomplete gamma functions, and the subscript 50 indicates the quantities for $H_0 = 50$ km s$^{-1}$ Mpc$^{-1}$. The faint magnitude limit for the luminosity function is taken to be $\sim$4 mag fainter than $M^*$ corresponding to $\beta = 0.02522$ (Tinsley 1977).

To determine a shape of luminosity function for field galaxies, various authors have derived two parameters $\alpha$ and $M^*_{B_J}$ which are highly correlated to each other. We here adopt the values of $(\alpha, M^*_{B_J}) \sim (-1.11, -21.1)$ for $H_0 = 50$ km s$^{-1}$ Mpc$^{-1}$ (Table 2). Since the available data of field galaxies are not sufficient to define the luminosity function of each galaxy type, we assume that the shape of luminosity function is independent of type in the $B_J$ band.[3] A reasonable dependence of $\alpha$ and $M^*_{B_J}$ on type and its effect on the galaxy number count were discussed in Bruzual and Kron (1980) and Ellis (1983).

The value of $\varphi^*_{50}$ is chosen to reproduce the observed count

[3] Tammann, Yahil, and Sandage fitted the Schecter function to the galaxies of each type in the Shapley-Ames catalog. They found that $M^*_{B_J}$ becomes monotonically brighter toward earlier types, while $\alpha$ bears no relation to the types.

TABLE 2

LOCAL PROPERTIES OF GALAXIES IN THE $B_J$ BAND ($\lambda_{B_J} = 4627$ Å) FOR $H_0 = 50$ km s$^{-1}$ Mpc$^{-1}$

| $\alpha$ | $M^*_{B_J}$ (mag) | $\varphi^*$ (gal Mpc$^{-3}$) | $n_0$ (gal Mpc$^{-3}$)[a] | $\mathscr{L}_0$ ($10^7$ $L_\odot$ Mpc$^{-3}$)[a] | $I_0$[b] | References |
|---|---|---|---|---|---|---|
| −1.11 | −21.1 | $1.4 \times 10^{-3}$ | $5.4 \times 10^{-3}$ | 5.5 | 1.54 | E |
| −1.11 | −21.1 | $2.3 \times 10^{-3}$ | $8.9 \times 10^{-3}$ | 9.0 | 2.52 | KOS(adopted) |
| −1.25 | −21.28 | $2.2 \times 10^{-3}$ | $1.1 \times 10^{-2}$ | 11.2 | 3.14 | F |
| −1.25 | −21.1 | $5.0 \times 10^{-3}$ | $2.6 \times 10^{-2}$ | 21.5 | 6.02 | S |

[a] The local densities $n_0$ and $\mathscr{L}_0$ are evaluated using $M_{B_J\odot} = 5.34$ mag, $[\Gamma(1+\alpha,\beta), \Gamma(2+\alpha,\beta)] = (3.880, 1.035)$ for $(\alpha, \beta) = (-1.11, 0.02522)$, and $(5.219, 1.142)$ for $(\alpha, \beta) = (-1.25, 0.02522)$.

[b] The normalization $I_0$, in units of $10^{-5}$ ergs s$^{-1}$ $\mu$m$^{-1}$ cm$^{-2}$ sr$^{-1}$, to the EBL is evaluated using $L_\odot \sim 5.58 \times 10^{33}$ ergs s$^{-1}$ $\mu$m$^{-1}$ at $\lambda \sim 0.46$ $\mu$m (Allen 1973).

REFERENCES.—E, Ellis 1983; KOS, Kirschner, Oemler and Schechter 1979; F, Felten 1977; S, Schechter 1976.

of galaxies at bright magnitudes. The value $\varphi^*_{50} = 2.3 \times 10^{-3}$ galaxies Mpc$^{-3}$ adopted here gives a satisfactory fit to the count over the range of $B_J = 12$–16 mag, corresponding to $A(B_J) = 0.5$ galaxies deg$^{-2}$ in a half-magnitude interval centered on $B_J = 15$ mag. The local number density $n_0$ and the local luminosity density $\mathscr{L}_0$ in the $B_J$ band are tabulated in Table 2, together with the values of other authors. (The galaxy count data have usually been obtained in the $B_J$ and $R_F$ bands which are slightly different from those of the Johnson 1966 system. Eqs. [2], [4], and [5] of Shanks *et al.* 1984 transform the Johnson $B$ and $R$ magnitudes into the $B_J$ and $R_F$ magnitudes via $B_J = B - 0.18$ mag and $R_F = R + 0.15$ mag using the average galaxy colors weighted by the proportion of each type; $B - V = 0.77$ mag and $V - R = 0.77$ mag.)

In evaluating the $K$ correction defined in equation (3) for each galaxy type, the present-day spectral energy distribution (SED) and the sensitivity function $R_\lambda(\lambda')$ are necessary. The references for the functions $R_\lambda(\lambda')$ in various magnitude systems are summarized in Table 4 of Bruzual (1983*a*). The SEDs in the ultraviolet ($\lambda < 0.3$–0.4 $\mu$m), the optical ($\lambda \sim 0.4$–1 $\mu$m), and the infrared ($\lambda > 1$ $\mu$m) regions have been obtained by different observational techniques. The sources for the observed SEDs at $\lambda < 1$ $\mu$m are tabulated in Table 3. The optical SED for each galaxy type is based on spectrophotometry of galaxies and gives a reliable $K$ correction. For the purpose of determining the $K$ correction at fairly large redshift the ultraviolet SEDs are taken from either broad-band *OAO 2* and *ANS* data or *IUE* data at high resolution 6 Å. For elliptical galaxies the broad-band satellite data agree well with the average *IUE* spectra in the range of $\lambda > 0.2$ $\mu$m (Bruzual and Spinrad 1981), but the *IUE* spectra below $\lambda \sim 0.2$ $\mu$m show an upturn feature due to the hot component in ellipticals. Among the *IUE* observations of E/S0 galaxies, NGC 4649 shows the highest ultraviolet energy flux. This galaxy has been observed also with *OAO 2*. Although the aperture of the *IUE* observation is enormously smaller than that of *OAO 2*, these two SEDs are quite similar as shown in Figure 1. Therefore, in the present paper we use the *IUE* data of NGC 4649 as a typical SED for E/S0. On the other hand, for spiral galaxies, we adopt the SED for Sab derived by Pence (1976) using *OAO 2* data, and the SED for late-type spirals by Coleman, Wu, and Weedman (1980) using *ANS* data.

The infrared SED for each galaxy type can be evaluated from the broad-band colors of ground-based observations tabulated in Table 4. The photometry of giant ellipticals has been performed in the *UBVRIJHKL* bands in the Johnson system, whereas mostly in the *UBVRK* bands for spirals. To cover the range of wavelength to the $L$ band ($\lambda_L = 3.4$ $\mu$m), we

TABLE 3

DATA SOURCES OF SED OF GALAXIES IN ULTRAVIOLET AND OPTICAL REGIONS

| Type | Object | Range of $\lambda$ (Å) | Method[a] | References |
|---|---|---|---|---|
| E/S0 ..... | NGC 4649(E2) | 1255–3113 | *IUE*(15″) | BCO (Table 2) |
| | NGC 3379(E1) | 1264–3226 | *IUE*(15″) | OBC (Table 2) |
| | NGC 4649(E2) | 1550–4250 | *OAO 2*(10′) | CW (Table 1) |
| | NGC 4649(E2) | 3200–10760 | Hale telescope | BCO (Table 2) |
| Sab ..... | NGC 4736 | 1550–4250 | *OAO 2*(10′) | CWP } P (Table 3) |
| | NGC 1357 | 3500–5500 | McDonald Obs Telescope | W } |
| | NGC 3379(E1) | 5500–8000 | Mt Wilson Obs Telescope | OS } |
| Sbc ..... | M51, NGC 2903 | 1550–3300 | *ANS*(2.′5) | CWW } CWW (Table 3) |
| | NGC 470, 1659 | 3500–5500 | McDonald Obs Telescope | W } |
| | ... | 5500–10000 | Extrapolation | P } |
| Scd ..... | M33, NGC 2403 | 1550–3300 | *ANS*(2.′5) | CWW } CWW (Table 4) |
| | ... | 3500–10000 | Interpolation between Sbc and Sdm | P } |
| Sdm ..... | NGC 4449 | 1550–3300 | *ANS*(2.′5) | CWW } CWW (Table 5) |
| | NGC 1140 | 3500–5500 | McDonald Obs Telescope | W } |
| | ... | 5500–10000 | Extrapolation | P } |

[a] The aperture for the satellite observations is given in the parentheses.

REFERENCES.—CW, Code and Welch 1979; BCO, Bertola, Capaccioli, and Oke 1982; OBC, Oke, Bertola, and Capaccioli 1981; CWP, Code, Welch, and Page 1972; W, Wells 1972; OS, Oke and Sandage 1968; P, Pence 1976; CWW, Coleman, Wu, and Weedman 1980.

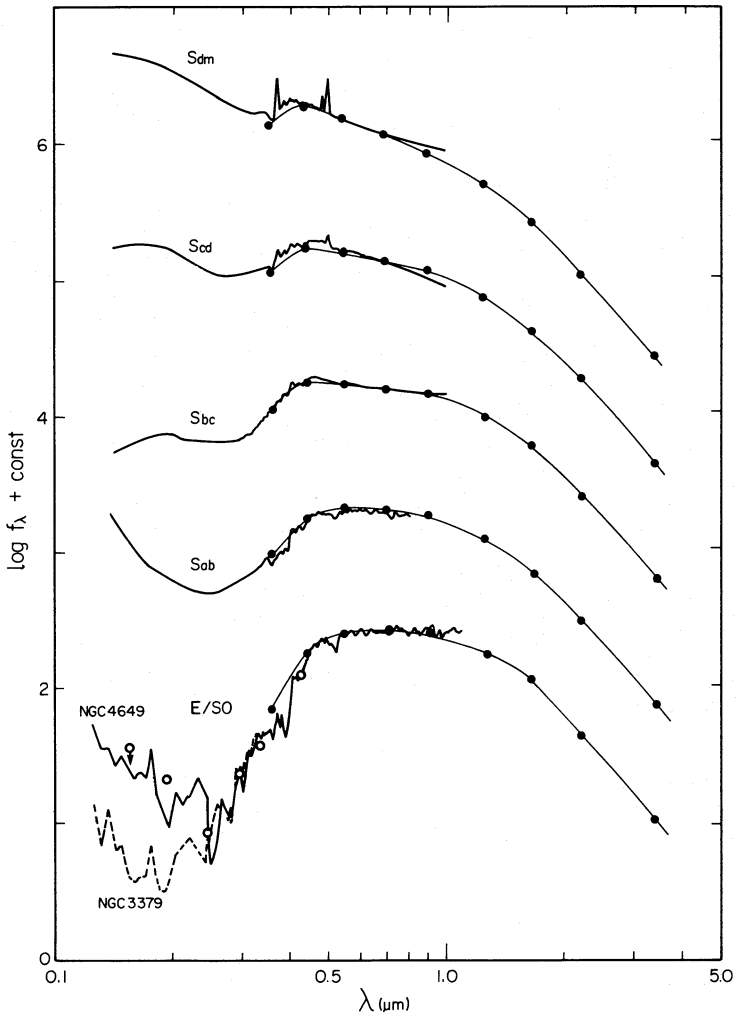


FIG. 1.—Present-day spectral energy distribution (SED) for each galaxy type of E/S0, Sab, Sbc, Scd, and Sdm. Scale of the ordinate is arbitrary. Thick lines represent the observed SEDs. Filled circles represent the fluxes in the Johnson *UBVRIJHKL* bands synthesized by Arimoto and Yoshii (1986, 1987). Observed and synthesized SEDs are made to coincide with each other at $\lambda_R = 0.7$ $\mu$m. For the ultraviolet SED of NGC 4649, thick line corresponds to the *IUE* data and open circles to the *OAO 2* data. In the present paper we use the *IUE* SED of NGC 4649 for E/S0 galaxies. The *IUE* SED of NGC 3379 is shown only for the purpose of comparison.

use the model spectra which are filled to the observed colors of different galaxy types (Arimoto and Yoshii 1986, 1987). The synthesized colors in the *UBVRIJHKL* bands are tabulated in Table 4. Linking the observed and synthesized SEDs smoothly at $\lambda_R = 0.7$ $\mu$m, we construct the composite SED in the range of $\lambda \sim 0.1$–3.4 $\mu$m for each of E/S0, Sab, Sbc, Scd, and Sdm (Fig. 1).

### c) *Evolution of Galaxies*

In evaluating the $E$ correction defined in equation (4), the evolving SED is necessary for each galaxy type. Arimoto and Yoshii (1986, 1987) constructed the models of population synthesis which are consistent with chemical evolution. Using three parameters such as a constant coefficient $\nu$ of star formation rate (SFR) per unit mass, a power index $\mu$ of the initial stellar mass function (IMF), and a cutoff time $t_{cut}$ for star formation due to gas removal by a galactic wind, they computed luminosity evolution of galaxies in Johnson *UBVRIJHKL* magnitudes up to the age of $T_G = 15$ Gyr in the rest frame. While the models for spirals are constructed without star formation cutoff, the present-day SED of ellipticals is reproduced by stopping star formation at an early epoch.

The parameters ($\nu$, $\mu$, $t_{cut}$) of the models representative of E/S0, Sab, Sbc, Scd, and Sdm are tabulated in Table 4. For E/S0 galaxies we use a wind model with $M_G = 10^{12}$ $M_\odot$ although their evolution possibly depends on $M_G$. (Bruzual 1983*a* and Bruzual and Kron 1980 modeled the evolving SED assuming that stars are formed at an exponentially decreasing rate [$\mu_B$ model; $\mu_B$ is the mass fraction of stars formed in the first 1 Gyr] or at a constant rate within the first 1 Gyr [c model]. For the purpose of comparison, we note that Arimoto and Yoshii models correspond to the $\mu_B$ model for spirals, where $\mu_B$ is related to $\nu$ via $\mu_B = 1 - \exp(-0.15\nu)$, and to the c model for ellipticals.) It should be noted that the evolutionary brightening of E/S0 is more prominent in the passbands of shorter wavelengths and that such luminosities attain a maximum in more remote past than the infrared luminosities. Similar tendency holds for Sabc, but with smaller maximum luminosity in each passband. On the other hand, the evolution makes Scdm dim monotonically in the past. Figure 2 shows the

TABLE 4

EMPIRICAL (E) AND MODEL (M) COLORS OF PRESENT GALAXIES

| Type | E/M | $U-B$ | $B-V$ | $U-V$ | $V-R$ | $V-I$ | $V-J$ | $V-H$ | $V-K$ | $V-L$ | References |
|---|---|---|---|---|---|---|---|---|---|---|---|
| E/S0 ..... | E | 0.54 | 0.96 | 1.50 | 0.84 | 1.59 | 2.37 | ... | 3.31 | ... | Tb |
| | E | ... | 0.97 | ... | 0.86 | 1.61 | 2.20 | ... | 3.20 | ... | TG |
| | E | ... | ... | 1.40 | ... | ... | ... | ... | 3.22 | ... | A |
| | E | 0.58 | 0.97 | ... | 0.89 | 1.70 | 2.47 | ... | 3.39 | 3.56 | W |
| | E | ... | ... | 1.33 | ... | ... | 2.36 | 3.05 | 3.26 | ... | FPAM |
| | M | 0.61 | 1.02 | 1.63 | 0.94 | 1.79 | 2.38 | 2.90 | 3.25 | 3.44 | AYb; (45.0, 0.95, 0.71)[a] |
| Sab ..... | E | 0.10 | 0.79 | 0.89 | 0.86 | ... | ... | ... | ... | ... | Ta |
| | E | ... | ... | 1.07 | ... | ... | ... | ... | 3.18 | ... | A |
| | M | 0.13 | 0.79 | 0.92 | 0.83 | 1.57 | 2.10 | 2.62 | 2.94 | 3.11 | AYa; (1.58, 1.35, ∞)[a] |
| Sbc ..... | E | −0.09 | 0.64 | 0.55 | 0.66 | ... | ... | ... | ... | ... | Ta |
| | E | ... | ... | 0.71 | ... | ... | ... | ... | 3.06 | ... | A |
| | M | −0.06 | 0.64 | 0.58 | 0.77 | 1.51 | 2.03 | 2.56 | 2.90 | 3.07 | AYa; (0.68, 1.35, ∞)[a] |
| Scd ..... | E | −0.17 | 0.54 | 0.37 | 0.62 | ... | ... | ... | ... | ... | Ta |
| | E | ... | ... | 0.45 | ... | ... | ... | ... | 2.74 | ... | A |
| | M | −0.14 | 0.56 | 0.42 | 0.70 | 1.36 | 1.85 | 2.36 | 2.68 | 2.85 | AYa; (0.25, 1.35, ∞)[a] |
| Sdm ..... | E | −0.15 | 0.52 | 0.37 | 0.53 | ... | ... | ... | ... | ... | Ta |
| | E | ... | ... | 0.23 | ... | ... | ... | ... | 2.32 | ... | A |
| | M | −0.17 | 0.46 | 0.29 | 0.57 | 1.03 | 1.40 | 1.81 | 2.05 | 2.19 | AYa; (0.01, 1.35, ∞)[a] |

[a] $(\nu, \mu, t_{cut})$: the SFR is proportional to the gas mass, i.e., $dM_{star}/dt = \nu M_{gas}$. The value of $\nu$ is normalized by the solar neighborhood value $\nu_0 = 6.08 \times 10^{-18}$ s$^{-1}$. The IMF is expressed as $dn/dm \propto m^{-(1+\mu)}$, and the stellar mass range is fixed to be 0.05 $M_\odot < m < 60\ M_\odot$. For early-type galaxies E/S0 the star formation is assumed to cease at the cutoff time $t_{cut}$ due to gas removal by a galactic wind. The value of $t_{cut}$ is in units of Gyr.

REFERENCES.—Ta, Tinsley 1978*a*; Tb, Tinsley 1978*b*; TG, Tinsley and Gunn 1976; A, Aaronson 1978; W, Whitford 1977; FPAM, Frogel *et al.* 1978; AYa, Arimoto and Yoshii 1986; AYb, Arimoto and Yoshii 1987.

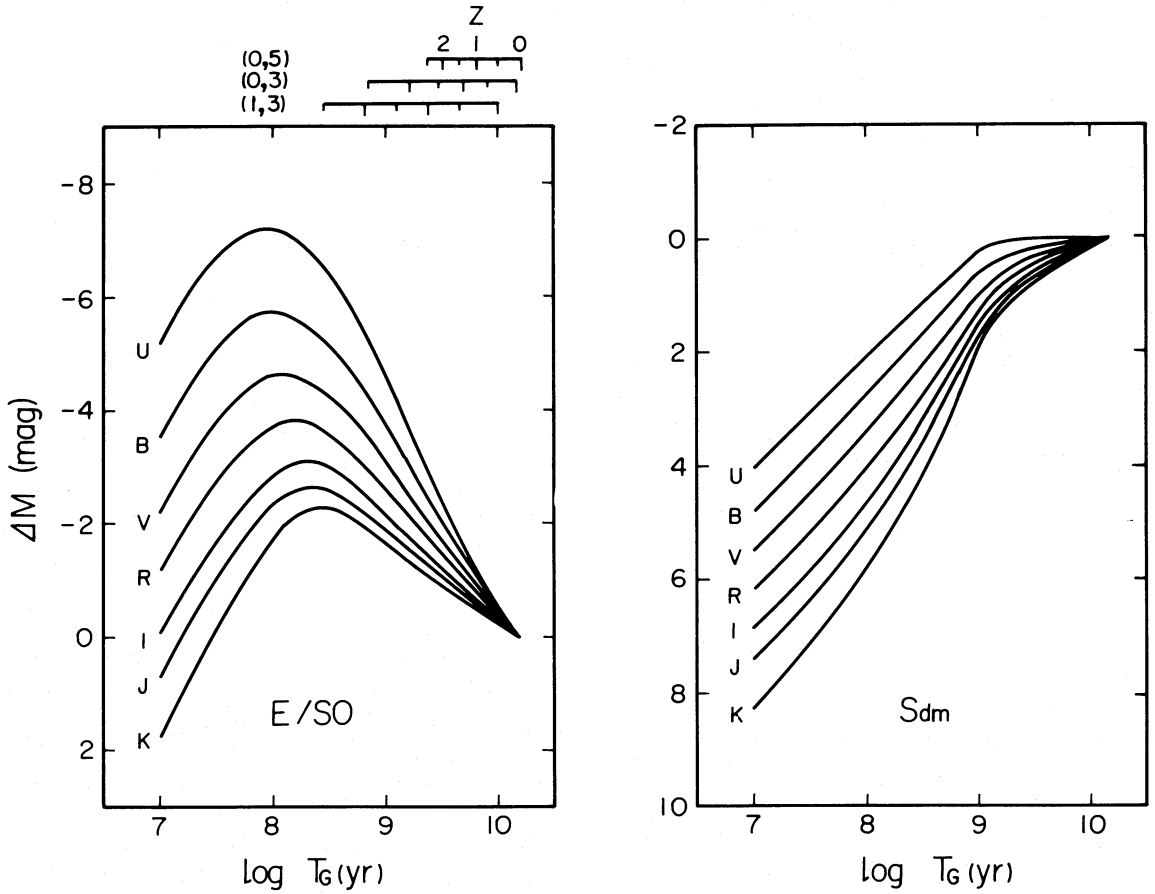


FIG. 2.—Evolutions of absolute *UBVRIJKL* magnitudes in the Johnson system computed by Arimoto and Yoshii (1986, 1987). The magnitudes are relative to those at $T_G = 15$ Gyr for (*a*) E/S0 and (*b*) Sdm. The redshift corresponding to a given age of galaxies is indicated above the upper abscissa for various values of $(q_0, z_F)$.

evolutions of the *UBVRIJK* magnitudes relative to those at $T_G = 15$ Gyr for E/S0 and Sdm. As shown in this figure, the magnitudes in various passbands change linearly with log $T_G$ at $T_G > 10$ Gyr, so that we may extrapolate those curves beyond $T_G = 15$ Gyr. The galactic age $t_G(0)$ defined in equation (8) is not always equal to 15 Gyr; for example, $t_G(0) = 10$ Gyr for $(q_0, z_F) = (1, 3)$ and 16 Gyr for (0, 5). Since the difference between the magnitudes at $T_G = 10$ Gyr and 16 Gyr is less than 0.4 mag, the shape of SED remains almost unchanged in this period. Therefore, we take the magnitude at $T_G = t_G(0)$ as the present-day magnitude. This approximation introduces no serious change in the result because the difference $|\Delta M| \sim 0.4$ mag from $T_G \sim 10$ Gyr to 16 Gyr is much smaller than the $E$ correction at redshift of interest ($z > 0.5$).

The evolving SED covers a range of wavelength longer than $\lambda_U (= 0.36\ \mu\text{m})$, so that the $E$ correction can be calculated up to $z = 0.2(B), 0.5(V), 0.9(R), 1.5(I), 2.5(J), 5.1(K), 3.6(H)$, and $8.4(L)$ for each passband indicated in the parentheses. For higher redshift than above we approximate the $E$ correction at an effective wavelength $\lambda$ as

$$E_\lambda(z) = -2.5 \log \frac{f_{\lambda_U}(z)}{f_{\lambda_U}(0)} \qquad \left(z > \frac{\lambda}{\lambda_U} - 1\right). \tag{12}$$

This assumes that the evolving SED below $\lambda_U$ keeps the same shape as the present-day SED $f_\lambda(0)$ and scales with the flux at $\lambda_U$.[4] It is evident that more realistic estimate of the $E$ correction is necessary especially in the optical passbands. The Bruzual $\mu_B$ and c models may serve for this purpose because the evolving SED is extended down to $\lambda \sim 0.12\ \mu$m. In his models, the ratio $f_\lambda(z)/f_{\lambda_U}(z)$ at a given $z$ becomes larger toward shorter wavelength from $\lambda_U$ (see also Tinsley 1973). Therefore, our $E$ correction in equation (12) is possibly underestimated. This underestimate may be serious especially for elliptical galaxies in the study of magnitude-redshift relation (§ III) and of the galaxy number count at faint magnitudes where elliptical galaxies dominate in number (§ IV). The Bruzual c model which is more appropriate to ellipticals fails to reproduce their observed UV light excess. As an alternative, the $\mu_B = 0.5$–$0.7$ models have often been used for ellipticals because the UV light from AF main-sequence stars mimics the upturn SED feature below $\lambda \sim 0.2\ \mu$m (Bruzual 1983*a*). However, a possible source of the UV light in ellipticals is considered to be horizontal branch (HB) stars (e.g., Aaronson, Cohen, and Mould 1978; Bruzual 1983*a*; Arimoto and Yoshii 1987). Since the present knowledge on the evolutionary stage of HB stars is highly incomplete, Bruzual (1983*a*) examined in a very crude way the effect of including HB stars in the c model. He showed that inclusion of HB stars brightens the $E$ correction approximately by 1 mag in the $B_J$ band and 0.5 mag in the $V$ band at $z > 1$ (see Tables 17 and 18 of Bruzual 1983*b*). This may indicate a range of not only the underestimate of our $E$ correction but also of the uncertainty involved in all current models of ellipticals until HB stars will be incorporated properly in the evolutionary synthesis of stellar population. Keeping above uncertainty in mind, we will investigate the effect of luminosity evolution of galaxies in the subsequent sections.

[4] Since $f_\lambda(0)$ has been fitted to the observed SED shown in Fig. 1, our model for ellipticals is similar to the Bruzual c model modified by Lilly and Longair (1984).

## III. MAGNITUDE AND COLOR VERSUS REDSHIFT RELATION

The first-ranked or brightest galaxies in clusters with different redshifts are assumed to be giant ellipticals. Given the absolute magnitude of giant ellipticals as standard candles, their apparent magnitudes are derived as a function of $z$ with prescribed values of $q_0$ and $z_F$. Therefore, the observed $m-z$ relation in the so-called Hubble diagram is useful to determine the cosmological model as well as to detect the luminosity evolution of galaxies.

In general, the observed magnitudes corrected for the aperture-redshift relation with $q_0 = 1.0$ are plotted in the Hubble diagram. In the present paper, the apparent magnitude derived theoretically with a prescribed value of $q_0$ is transformed to the magnitude on the standard metric for $q_0 = 1.0$ by making use of Table 3 of Sandage (1972*a*). The standard metric diameter is adopted to be $86(H_0/50)^{-1}$ kpc which corresponds roughly to the apertures used for the observations. Since the growth curve in the $V$ magnitude (Sandage 1972*a*) is similar to that in the $K$ magnitude (Frogel *et al.* 1978), we use the growth curve in the $V$ magnitude irrespective of passband.

The absolute magnitude of galaxies at $z \sim 0$ should be determined such that the theoretical $m-z$ relation coincides with the observed relation at the bright magnitude limit where both the $K$ and $E$ corrections are small. The absolute magnitudes determined here are $M_V = -23.2$ mag and $M_K = -25.3$ mag for $H_0 = 50\ \text{km s}^{-1}\ \text{Mpc}^{-1}$.

### *a) Magnitude versus Redshift Relation*

#### *i) $V_{SM} - z$ Relation*

Figure 3 shows the $V_{SM} - \log z$ relation where $V_{SM}$ indicates the apparent $V$ magnitude corrected to the standard metric. Over the range of redshift in this figure the model without the $E$ correction depends on only $q_0$, whereas the model with the $E$ correction depends on both $q_0$ and $z_F$. The thick and thin lines represent the models with and without the $E$ correction, respectively. The numbers beside the lines indicate the values of the parameters. As shown in the figure, the linearity of the $V_{SM} - \log z$ relation breaks down at $z \sim 0.2$. For larger $z$ the $K$ dimming works, and the $V_{SM}$ magnitude becomes fainter than that by extrapolation of the $V_{SM} - \log z$ relation defined at $z < 0.2$. The $K$ dimming amounts to $\sim 4$ mag at $z \sim 1$. As $q_0$ increases, the luminosity distance $d_L$ decreases monotonically. Therefore, the $V_{SM}$ magnitude at a given $z$ becomes brighter for larger $q_0$. However, even at $z \sim 2$, the $V_{SM}$ magnitude for $q_0 = 1.0$ is brighter than that for $q_0 = 0.02$ by only 1 mag in the no evolution model.

We here consider the effect of luminosity evolution on the $m-z$ relation. Since the model elliptical galaxy evolves through an epoch of maximum luminosity (Fig 2*a*), the evolutionary brightening becomes comparable to the effect of the $K$ dimming. For a given $z$, the age $t_G(z)$ of a galaxy decreases with increasing $q_0$ or with decreasing $z_F$, and the epoch of maximum luminosity comes into sight in more recent past. Therefore, the evolutionary brightening increases with increasing $q_0$ or with decreasing $z_F$, as shown in Figure 3. There appears a characteristic magnitude at $z > 1$ where the $V_{SM}$ magnitude becomes insensitive to $z$, i.e., $V_{SM} \sim 24$ mag for $q_0 = 0.02$, 23 mag for $q_0 = 0.5$, and 22 mag for $q_0 = 1.0$; the effect of luminosity evolution shows up at $V_{SM} \sim 22$–$24$ mag. If galaxies at $z > 1$ have magnitudes in this range, it indicates an evidence that galaxies underwent the luminosity evolution.

The data of Kristian, Sandage, and Westphal (1978) give the

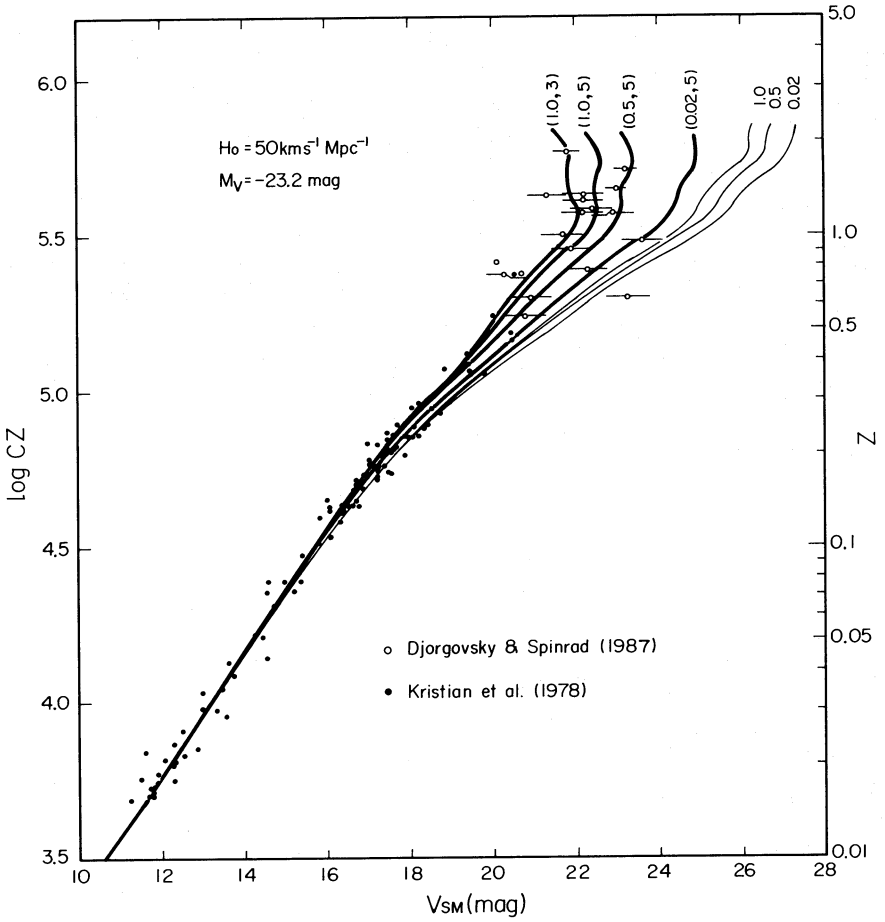


FIG. 3.—Magnitude vs. redshift diagram for standard candle galaxies in the $V$ band. The symbol $V_{SM}$ indicates that the apparent magnitudes are corrected to the standard metric using the aperture-redshift relation with $q_0 = 1.0$. Thick and thin lines represent the models for evolving and nonevolving galaxies, respectively. Number beside each thin line is the value of $q_0$, and numbers in parentheses beside each thick line are the values of $q_0$ and $z_F$. Data of radio galaxies by Djorgovski and Spinrad are shown only for $z > 0.5$.

$V$ magnitudes of the first-ranked cluster galaxies to which the $K$ correction has been applied. To compare them with the models where the $K$ correction is included, we rederived the observed magnitudes without the $K$ correction. The data thus rederived are shown in Figure 3. Since their data are confined within $z = 0.7$, it seems impossible to determine the value of $q_0$. Recently, Djorgovski and Spinrad (1987) derived the $V$ magnitudes of radio galaxies in the range of $0.4 < z < 1.8$. In fact, radio galaxies comprise a very small fraction of all elliptical galaxies and sometimes show peculiar colors. However, recent photometric studies reveal that they are most likely the distant giant ellipticals and are useful as standard candles in the cosmological study (e.g., Lilly and Longair 1984; Lebofsky and Eisenhardt 1986; Spinrad 1986). In the present paper, we simply assume that radio galaxies are giant ellipticals which have similar properties to the first-ranked cluster galaxies. The data of Djorgovski and Spinrad (1987) are also shown in Figure 3. The sample galaxies have almost a constant magnitude of $V_{SM} \sim 22$–$23$ mag over the range of $z$. This trend is clearly inconsistent with the no evolution models, as indicated by Djorgovski and Spinrad (1987). In other words, the evolution certainly shows up in distant galaxies. Comparison of the evolution models with the data indicates that the $V_{SM}$ magnitude-redshift relation favors high $q_0$ models. The $q_0 = 0.02$ model predicts the characteristic magnitude $V_{SM} \sim 24$ mag at $z > 1$, $\sim 2$ mag fainter than the observations, which is difficult to attain even if the underestimate ($\sim 0.5$ mag) of our $E$ correction is taken into account. One the other hand, the $q_0 = 0.5$ and 1.0 models are in reasonable agreement with the observations.

### ii) $K_{SM} - z$ Relation

Figure 4 shows the $K_{SM} - \log z$ relation. In this figure the linearity of the $K_{SM} - \log z$ relation extends up to $z \sim 1$, compared to $z \sim 0.2$ in the $V$ band. Since the infrared SED of ellipticals inclines steeply to shorter wavelength and then becomes flatter from $\lambda \sim 1$ $\mu$m (Fig. 1), the $K$ correction in the $K$ band (2.2 $\mu$m) has a negative and small value up to $z \sim 1$ and a positive value at $z > 1$. This explains why the $K$ dimming is not important at $z < 1$. Since the $E$ correction in the $K$ band can be evaluated up to $z \sim 5$ without knowledge of the ultraviolet SED, the evolution effect will be examined more convincingly in the $K$ band than in the $V$ band. As shown in Figure 4, the evolutionary brightening shows up at $z > 1$. Galaxies at $z = 2$ are brighter by 2–3 mag than those without luminosity evolution. The characteristic magnitude at $z > 1$ where $K_{SM}$ is insensitive to $z$ is, then, $K_{SM} \sim 18$ mag for $q_0 = 0.02$, 17 mag for $q_0 = 0.5$, and 16 mag for $q_0 = 1.0$.

The data in the $K$ band are available from Frogel *et al.* (1978), Grasdalen (1980), and Lebofsky (1981). Four field ellip-

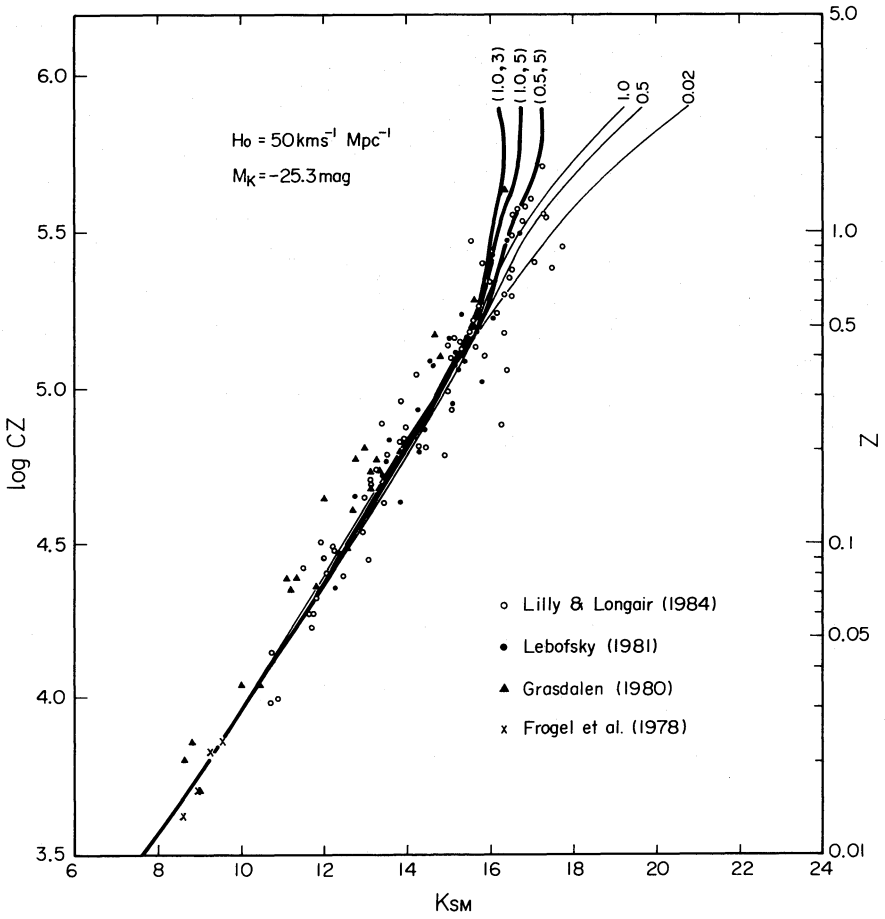


FIG. 4.—Magnitude vs. redshift diagram for standard candle galaxies in the $K$ band. The meanings of the theoretical lines are the same as in Fig. 3.

ticals with $z < 0.025$ in Frogel *et al.* (1978) are used to determine the absolute $K$ magnitude in the limit of small $z$. Most ellipticals in Grasdalen (1980) and Lebofsky (1981) are the first-ranked cluster galaxies. The data corrected for the aperture-redshift relation with $q_0 = 1.0$ and the Galactic extinction are plotted on the $K_{SM} - \log z$ plane in Figure 4. The former correction is applied to the data using the growth curve in the $V$ magnitude for the reason described above (Table 3 of Sandage 1972*a*), and the latter using the relation $A_K = 0.09A_V$ (Frogel *et al.* 1978) where $A_V$ is taken from Sandage (1972*b*). Lilly and Longair (1984) performed the infrared observations of radio galaxies. Applying the similar corrections we also plotted their data in Figure 4.

It is apparent from this figure that the distribution of the first-ranked cluster galaxies is not systematically different from the distribution of the radio galaxies (see Lebofsky and Eisenhardt 1986). At present, the large scatter in the observations reduces the advantage that modeling the Hubble diagram in the infrared passband does not suffer from the uncertain ultraviolet SED. We see in Figure 4 that the $q_0 = 0.02$ model without luminosity evolution predicts much fainter magnitudes at $z > 0.5$, and the $q_0 = 1.0$ model with evolution predicts much brighter magnitudes there. Consequently, these models are unfavorable. On the other hand, the $q_0 = 0.5$ model with evolution seemingly gives the best fit to the data provided $z_F \sim 5$. Lilly and Longair (1984) reached a similar conclusion by using their own evolution model. However, inspection of Figure 4 shows that the $q_0 = 0.5$ and 1.0 models without the evolution are also compatible with the observations. To discriminate better models, the observations of galaxies at $z \sim 2$ are still necessary.

### *b) Color versus Redshift Relation*

The color-redshift relation is formally given by

$$C_{1,2}(z) = C_{1,2}(0) + [K_1(z) - K_2(z)] + [E_1(z) - E_2(z)] , \quad (13)$$

where the color $C_{1,2}$ is defined as the difference between apparent magnitudes at wavelengths $\lambda_1$ and $\lambda_2$ ($\lambda_1 < \lambda_2$). The color-redshift relation without the term of $E$ corrections does not depend on either of $H_0$, $q_0$, or $z_F$. Therefore, whether or not the galaxies underwent luminosity evolution in the past can be examined more convincingly than by means of the magnitude-redshift relation.

#### i) $(B-V) - z$ Relation

Figure 5 shows the $(B-V) - z$ relation. The thick and thin lines represent the models with and without the $E$ correction, respectively. The ultraviolet SEDs ($\lambda < 0.3$ $\mu$m) of elliptical galaxies show different upturns toward shorter wavelength (Fig. 1). To see the uncertainty arising from the different ultraviolet SEDs, we show in Figure 5 the results on the basis of the SEDs of NGC 4649 and NGC 3379. The difference becomes significant at $z > 05$.

The term of the $E$ corrections shifts the color blueward as $z$ increases. The blueward shift becomes larger for larger $q_0$ and

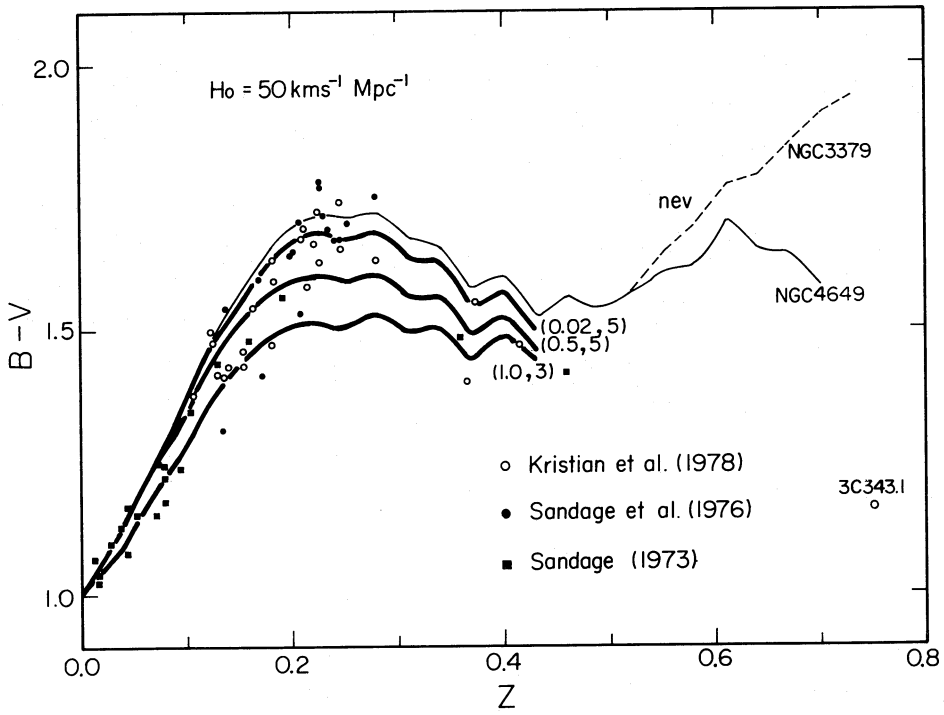


FIG. 5.—The $B-V$ color vs. redshift diagram for standard candle galaxies. The meanings of the theoretical lines are the same as in Fig. 3, but note that the nonevolving model denoted by "nev" does not depend on $H_0$, $q_0$, or $z_F$. The $(B-V)-z$ relation for the ultraviolet SED of NGC 3379 is shown only for the purpose of comparison.

amounts to $\sim 0.33$ mag at $z \sim 0.2$–0.3 for $q_0 = 1.0$. The approximation in equation (12) underestimates the blueward shift of $B-V$ color at $0.2 < z < 0.5$, and the term of $E$ corrections vanishes at $z > 0.5$ because the shape of the ultraviolet SED is assumed to be independent of $z$ in equation (12). Sandage (1973), Sandage, Kristian, and Westphal (1976), and Kristian, Sandage, and Westphal (1978) observed the $B-V$ colors of the first-ranked cluster galaxies. Their data are shown in Figure 5. The fact that the observed $B-V$ colors at $z > 0.3$ are bluer than the no evolution model suggests that ellipticals underwent spectral evolution and hence luminosity evolution in the past[5] although some part of blueward shift may be due to the aperture effect (Bruzual 1983*a*). It is unfortunate, however, that determination of $q_0$ is impossible owing to the uncertain $E$ corrections at $z > 0.2$.

ii) $(V-R)-z$ *Relation*

Figure 6 shows the $(V-R)-z$ relation. The trend of the relation is similar to that for the $B-V$ color. The blueward shift of the color from the no evolution model shows up at $z > 0.4$ for $q_0 = 0.02$, and at $z > 0.1$ for $q_0 > 0.5$. The color difference at $z \sim 0.5$ is $\sim 0.1$ mag for $q_0 = 0.02$, $\sim 0.3$ mag for $q_0 = 0.5$, and $\sim 0.4$ mag for $q_0 = 1.0$. The approximation in equation (12) underestimates the blueward shift of $R-V$ color at $0.5 < z < 0.9$. Sandage (1973), Sandage, Kristian, and Westphal (1976), and Kristian, Sandage, and Westphal (1978) observed the $V-R$ colors of the first-ranked cluster galaxies, and Djorgovski and Spinrad (1987) observed those of the radio galaxies. Their data are also shown in Figure 6. Their observed $V-R$ colors are bluer than the $q_0 = 0.02$ model with evolution. The $q_0 = 0.5$ and 1.0 models with evolution are compatible with the data at $z < 0.5$. However, the galaxies at much higher redshifts ($z > 0.5$) have the colors bluer than those of $q_0 = 1.0$. Therefore, more elaborate modeling of the $E$ correction at $z > 0.5$ is needed as far as the $V-R$ colors are concerned.

iii) $(H-K)-z$ *Relation*

Figure 7 shows the $(H-K)-z$ relation, for which the uncertain ultraviolet SED is not relevant to evaluation of infrared $E$ correction at redshifts of interest. The $H-K$ colors with luminosity evolution show a relatively weak dependence on $z$, because the low-energy tail of the SED is essentially similar to the Rayleigh-Jeans spectrum. A spread in the $H-K$ colors between the evolution and no evolution models depends on the validity of this approximation in the infrared region. In Arimoto and Yoshii models, the infrared light of ellipticals is dominated first by metal-poor red giants and then by metal-rich ones according to the chemical evolution of galaxies. Owing to the mixture of red giants with different effective temperatures, the evolutionary effect shows up already at $z > 0.5$ (Fig. 7), in contrast to Bruzual models where all stars are assumed to be formed with the solar metallicity.

The $H-K$ color data are available from the observations of the first-ranked cluster galaxies by Lebofsky (1981) and of radio galaxies by Lilly and Longair (1984). These data are shown in Figure 7. We see again in this figure that the distribution of the cluster galaxies is not different from that of the radio galaxies (see Lebofsky and Eisenhardt 1986). Unfortunately, owing to the large scatter in the $H-K$ colors ($\sim 0.5$ mag) we

[5] Spinrad (1980, 1986) derived a monotonical decrease of the amplitude of 4000 Å break with increasing $z$ for cluster and radio elliptical galaxies. This trend is interpreted as an evidence of spectral evolution of early-type galaxies (Bruzual 1983*a*). Recently, however, Hamilton (1985) claimed no spectral evolution using the 4000 Å break data of his own. The reason of this difference is not known although it may have arisen from the different sampling criteria (see the discussion by Spinrad 1986).

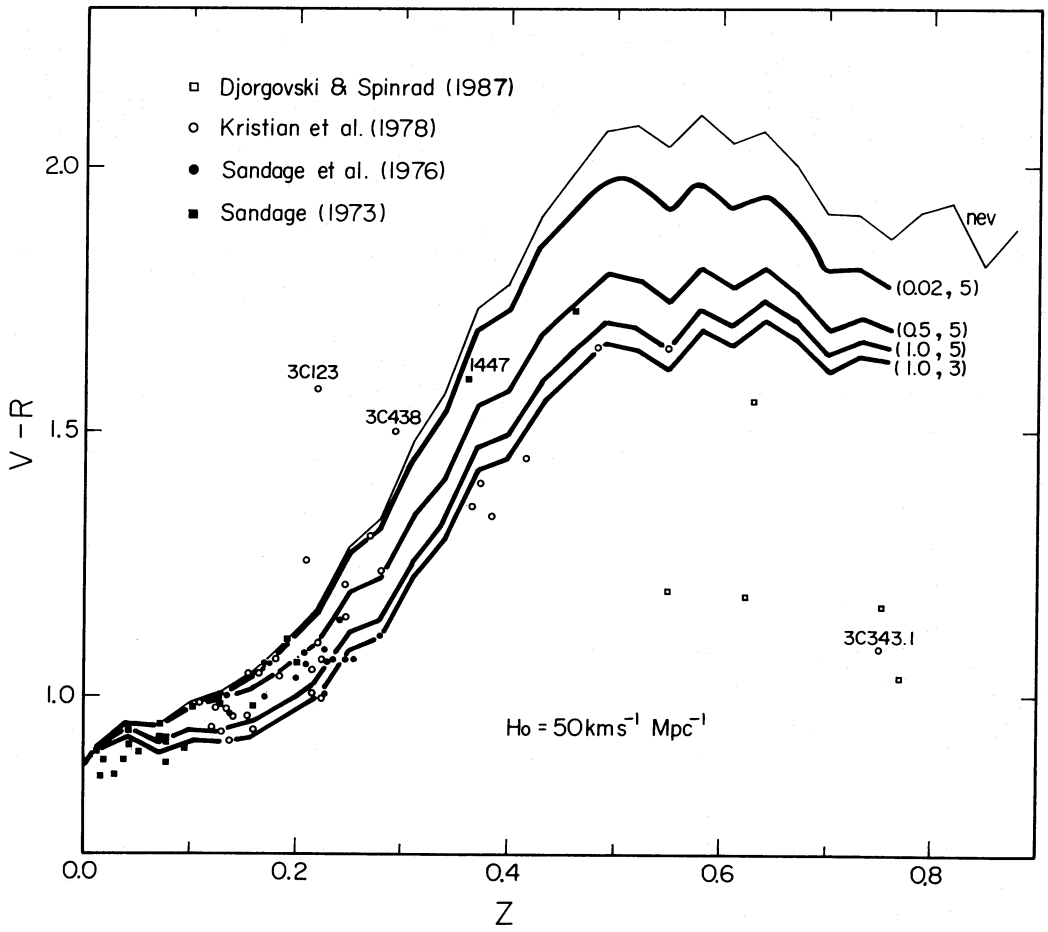


FIG. 6.—The $V-R$ color vs. redshift diagram for standard candle galaxies. The meaning of the theoretical lines are the same as in Fig. 5.

cannot constrain any spectral evolution nor the cosmological model.

## IV. GALAXY COUNT AND REDSHIFT DISTRIBUTION

The galaxy count data are obtained by counting up all images of galaxies on a finite area of the sky. Let $n(m_\lambda, z)dm_\lambda\, dz$ be the number of galaxies between $m_\lambda$ and $m_\lambda + dm_\lambda$ and between $z$ and $z + dz$, then we have

$$n(m_\lambda, z) = \frac{\omega}{4\pi}\frac{dV}{dz}\sum_{i=1}^{5}\psi^i(M_\lambda) \qquad (0 \le z \le z_F)\,, \qquad (14)$$

where $\omega$ is the angular area in units of steradians over which the galaxies are counted, and $\psi^i(M_\lambda)$ is the luminosity function for which the argument $M_\lambda$ is differently related to $m_\lambda$ depending on galaxy type $i$. Transforming $M_\lambda$ into $M_{B_J}$ via the color at $z = 0$, we evaluate $\psi^i(M_\lambda)$ from the luminosity function in the $B_J$ band, the shape of which is assumed to be independent of galaxy type (§ II*b*). Throughout this section, we adopt an area of 1 deg$^2$ ($\omega = 3.05 \times 10^{-4}$ sr).

### *a) Differential Number Count*

Integrating $n(m_\lambda, z)$ with respect to $z$, we have the differential number count:

$$n(m_\lambda) = \int_0^{z_F} n(m_\lambda, z)dz\,. \qquad (15)$$

The galaxy count data at very faint magnitudes have been obtained in the $B_J$ and $R_F$ bands. The model counts calculated in the Johnson $B$ and $R$ bands are shifted brightward by 0.18 mag and faintward by 0.15 mag, respectively (see § II*b*). In most cases the observed count is binned into a half-magnitude interval, whereas the typical rms error is $\sim 0.3$ mag. Therefore, we do not convolve this error because its effect on the model is not so significant (e.g., Shanks *et al.* 1984).

### *i) Count in the $B_J$ Band*

Figure 8 shows the differential number count in a half-magnitude interval in the $B_J$ band. The thick and thin lines represent the models with and without the $E$ correction, respectively, and the numbers beside the lines indicate the values of $q_0$ and $z_F$. At bright magnitudes where both the $K$ and $E$ corrections are not important, the count in logarithmic unit increases linearly with magnitude as $d \log n(m)/dm = 0.6$ because the homogeneous distribution of galaxies is assumed. As $B_J$ increases beyond 17 mag, the count increases less rapidly due to the effect of the $K$ dimming, reach a maximum, and then decreases monotonically. Such decline of $n(m)$ is caused by the decrease of the comoving volume toward larger redshift. The total number of galaxies becomes smaller for smaller $z_F$ because the comoving density of galaxies is assumed to be constant, and it does so for larger $q_0$ because the comoving volume is smaller. The magnitude at which the count begins to decline is sensitive to luminosity evolution of galaxies.

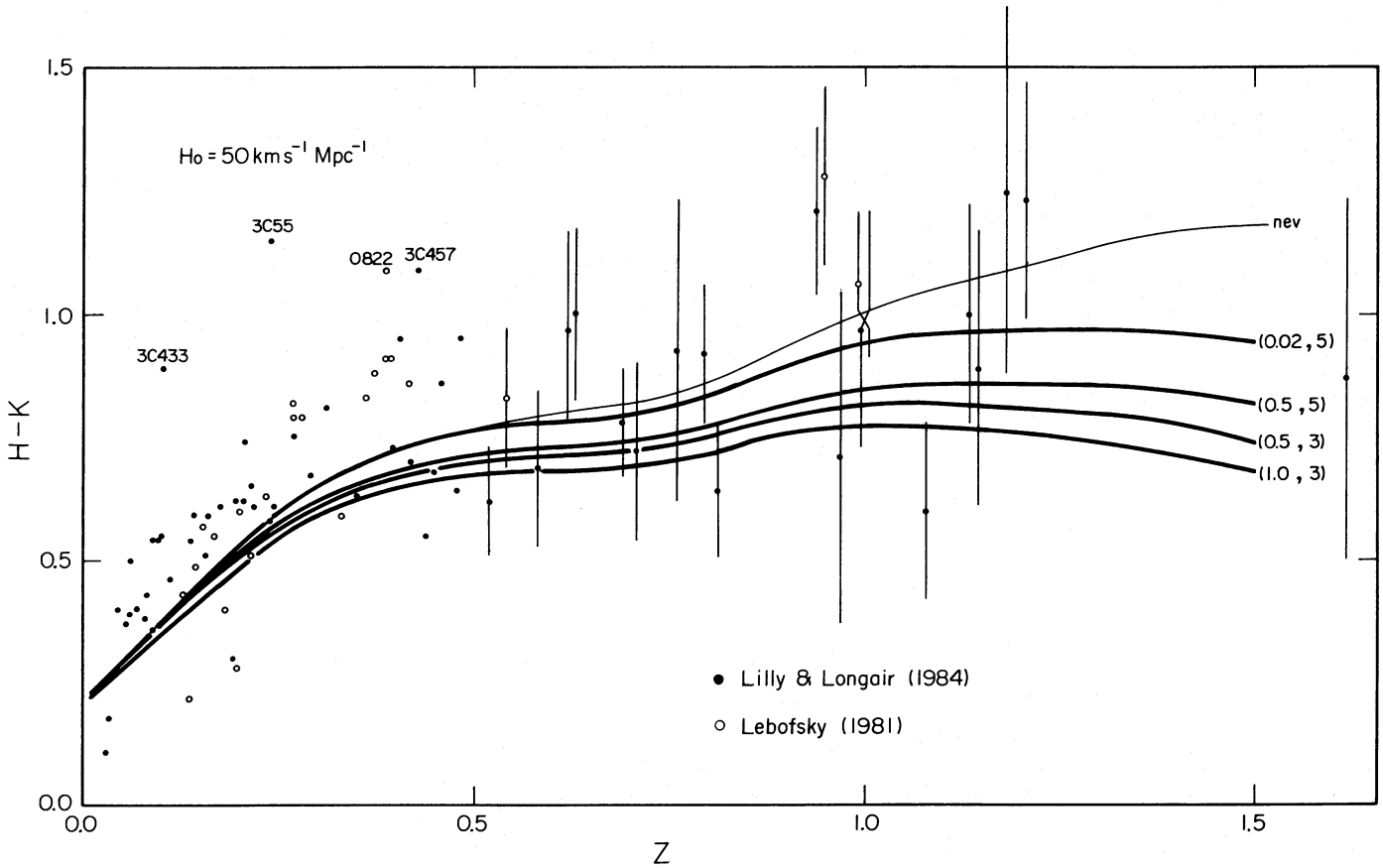


FIG. 7.—The $H-K$ color vs. redshift diagram for standard candle galaxies. The meaning of the theoretical lines are the same as in Fig. 5. Estimated errors in the color data are shown only for $z > 0.5$.

In the evolution models adopted here, E/S0 and Sabc galaxies in the rest frame are brighter, and Scdm galaxies are fainter in the past. Given $q_0$ and $z_F$, the evolutionary brightening of earlier galaxies shifts the magnitude brightward without changing the peak count appreciably. The converse is true for later galaxies. Since E/S0 and Sabc galaxies occupy a large fractional number in the local region (Table 1), the $\log n(m) - m$ relation becomes steeper and deviates significantly from the no evolution model at $B_J > 22$ mag. At fainter magnitudes, the count begins to flatten and then decline. The turnover in $\log n(m)$ occurs at $B_J \sim 28$–30 mag for $q_0 = 0.02$, 27–28 mag for $q_0 = 0.5$, and 26–27 mag for $q_0 = 1.0$, provided $z_F \sim 3$–5.

Figure 8 shows the blue counts at $B_J = 15$–17 mag taken from Kirshner, Oemler, and Schechter (1979) and Durham/AAT Redshift Survey (e.g., Fig. 2 of Ellis 1983), and the counts at $B_J = 17$–25 mag have been obtained by various authors (e.g., Peterson *et al.* 1979; Kron 1980; Jarvis and Tyson 1981; Shanks *et al.* 1984). The data of $B_J = 15$–17 mag are used to determine the constant $\varphi^*$ in the luminosity function (Table 2). As for the count data at fainter magnitudes, Kron (1980) and Jarvis and Tyson (1981) used the total magnitude scheme, while Peterson *et al.* (1979) and Shanks *et al.* (1984) used the isophotal magnitude scheme with the threshold at $\mu_{th} = 26.5$ mag arcsec$^{-2}$. Ellis (1980) pointed out that the total magnitude scheme fictitiously produces a steep rise in the count near the faint limiting magnitude. From Figure 8 we see a scatter in the counts with the different magnitude schemes as well as a scatter in the counts of different sources even if the same magnitude scheme is employed. The counts by all the other authors, including Kron (1980), fall in this range of uncertainty.

Contrary to the situation in the magnitude-redshift relation, the galaxy number count favors low $q_0$ models, as seen in Figure 8. The model count at $B_J = 25$ mag with luminosity evolution is $\log n(m) \sim 4.1$–4.4 for $q_0 = 0.02$, 4.1 for $q_0 = 0.5$, and 4.0 for $q_0 = 1.0$, compared to the observed count 4.3–4.6. The peak of the model count for $z_F = 5$ is $\log n_{peak} \sim 5.2$ for $q_0 = 0.02$, 4.5 for $q_0 = 0.5$, and 4.1 for $q_0 = 1.0$. The peak count for $q_0 = 1.0$ is far smaller than the observed count at $B_J = 25$ mag. Therefore, the $q_0 = 1.0$ model is highly unfavorable, because the luminosity evolution does not change the total number of galaxies for given $q_0$ and $z_F$.[6] On the contrary, the $q_0 = 0.02$ model with evolution resides within the scatter of the observed counts. The evolutionary brightening is not enough to shift the $q_0 = 0.5$ model into this scatter. Here it should be reminded that our $E$ correction in the $B_J$ band is possibly underestimated by $\sim 1$ mag at $z > 1$ (§ IIc). Since such high-redshift galaxies dominate in number at $B_J > 24$–25 mag, the

[6] The peak count is dependent on a shape of luminsity function at faint magnitudes. We have adopted the Schecter function truncated on the fainter side of $M = M^* + 4$ mag (§ II*b*). Recently, using the galaxies in the Virgo cluster, Sandage, Binggeli, and Tammann (1985) found that the luminosity function is bounded at the bright and faint, limits, close to a Gaussian form. Although their result may not be applicable to field galaxies, apparently the decline toward faint magnitude does not save the $q_0 = 1$ model.

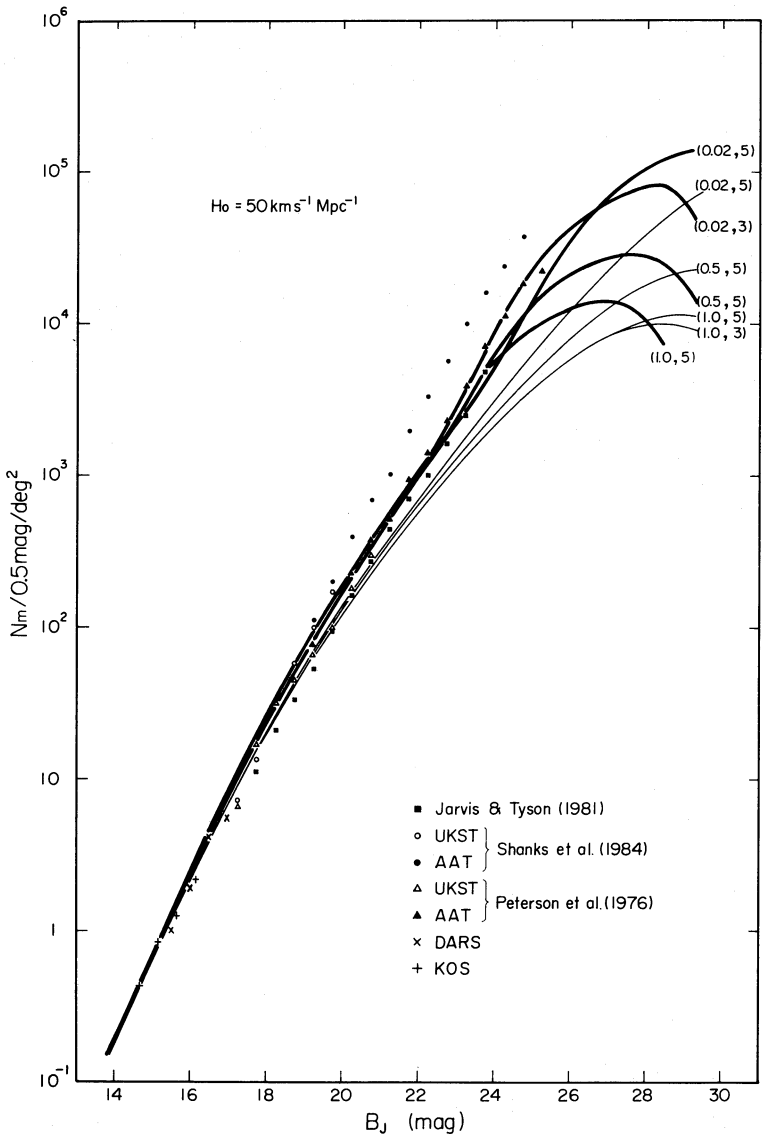


FIG. 8.—Differential number count of galaxies in the $B_J$ band in a half-magnitude interval in a unit area of 1 deg$^2$. Thick and thin lines represent the models for evolving and nonevolving galaxies, respectively. Numbers in parentheses beside each line are the values of $q_0$ and $z_F$.

$q_0 = 0.5$ model seems to be consistent with the observations. Using Kron's (1980) data, Bruzual and Kron (1980) concluded that the $q_0 = 0$ model is more favorable than the $q_0 = 0.5$ model. However, if the observational uncertainty is taken into account, it may be safe to conclude that $0 < q_0 < 0.5$ is an allowable range.

ii) *Count in the $R_F$ Band*

Figure 9 hows the differential number count in the $R_F$ band. The general trend of the model count with $q_0$ and $z_F$ is essentially the same as that in the $B_J$ band. However, the slope of the log $n(m) - m$ relation without luminosity evolution is substantially flatter than the same relation in the $B_J$ band. This occurs due to larger $K$ correction in the $R_F$ band, because the optical SED of nearby galaxies declines steeply toward shorter wavelength. Owing to the evolutionary brightning, the log $n(m) - m$ relation deviates significantly from the no evolution model at $R_F > 21$ mag. The count has a broad maximum at $R_F \sim$ 26–29 mag for $q_0 = 0.02$, ~25–28 mag for $q = 0.5$, and ~24–27 mag for $q_0 = 1.0$. The difference between the peak count for $q_0 = 0.02$ and that for $q_0 = 1.0$ amounts to $\Delta \log n_{\rm peak} \sim 1.1$ for $z_F = 5$, similar to the case in the $B_J$ band.

In most cases the red counts have been obtained at magnitudes brighter than $R_F = 23$ mag (e.g., Shanks *et al.* 1984; Couch and Newell 1984). The data taken from Shanks *et al.* (1984) are shown in Figure 9. For the similar reason in the $B_J$ count, the $q_0 = 0.02$ and 0.5 models with evolution are favorable, as indicated by Shanks *et al.* (1984). Recently, Hall and Mackey (1985) performed the CCD observations in a very small area of 0.0084 deg$^{-2}$ and obtained the red counts to the limit of 25 mag. Their data are also shown in Figure 9. (In plotting the CCD data, the $KG$ 3 magnitude is transformed into the $R_F$ magnitude via $R_F = KG\ 3 - 0.28$ mag.) The decline at $R_F > 24.5$ mag is due to the incompleteness of image detection. The model count at $R_F \sim 24$ mag with luminosity evolution is log $n(m) \sim 4.2$ for $q_0 = 0.02$, 4.1 for $q_0 = 0.5$, and 3.9 for $q_0 = 1.0$, compared to the observed count ~4.4. Therefore, the $q_0 = 1.0$ model is highly unfavorable, although faint

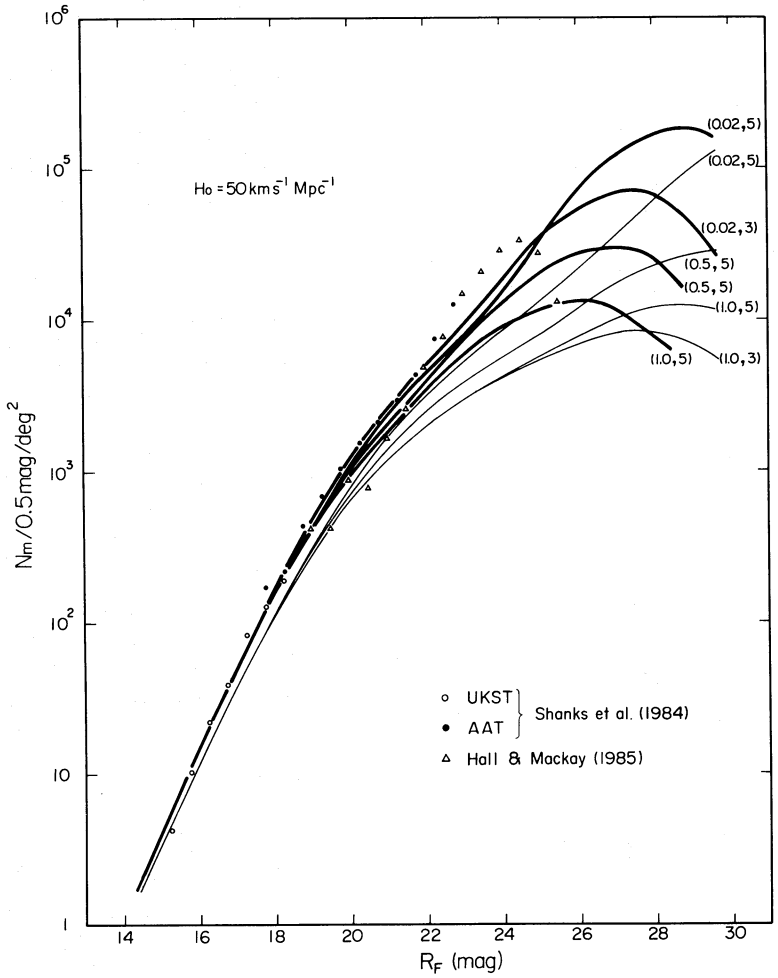


FIG. 9

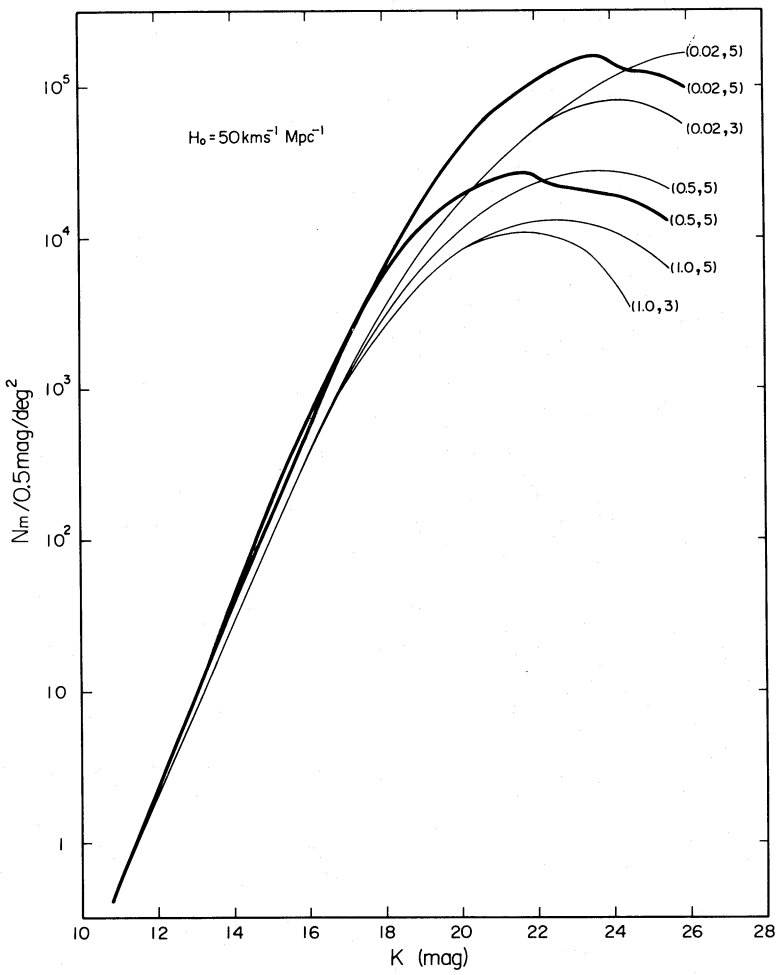


FIG. 10

FIG. 9.—Differential number count of galaxies in the $R_F$ band in a half-magnitude interval in a unit area of 1 deg$^2$. The meaning of the theoretical lines are the same as in Fig. 8. The decline in Hall and Mackay's count at $R_F > 24.5$ mag is due to the incompleteness of image detection.

FIG. 10.—Differential number count of galaxies in the $K$ band in a half-magnitude interval in a unit area of 1 deg$^2$. The meaning of the theoretical lines are the same as in Fig. 8.

galaxies should be counted over much larger area to minimize statistical fluctuations.

iii) *Count in the K Band*

We calculated the differential number count in the $K$ band, and the models are shown in Figure 10. The $K$ corrections for all types remain small at $z < 1$ until the optical SED is redshifted to the $K$ band. As shown in Figure 2, the evolutionary brightening of E/S0 and Sabc is smaller and the evolutionary dimming of Scdm is larger in the passband of longer wavelength. For this reason, the net $E$ correction is small in the $K$ band, so that the log $n(m) - m$ relation with luminosity evolution does not deviate significantly from the no evolution model. Therefore, the galaxy count in the $K$ band will give more sensitive test to determine the value of $q_0$, particularly, at $K \sim 20$–$22$ mag.

### b) *Redshift Distribution in the $B_J$ Band*

The redshift distribution for a magnitude-limited sample of galaxies illuminates the effect of luminosity evolution of galaxies (Tinsley 1977, 1980). Taking a case of $z_F = 3$, we show in Figure 11 the number count of galaxies binned into a logarithmic interval of redshift $\Delta \log z = 0.07$ for two magnitude ranges of $B_J = 22$–$23$ mag and 23–24 mag. The thick and thin lines indicate the evolution and no evolution models, respectively. The redshift distribution for nonevolving galaxies has a single maximum around $z \sim 0.3$ and falls off sharply toward larger redshift, while the distribution for evolving galaxies has two maxima on either sides of the break at $z \sim 1$; one is a broad maximum for low-redshift galaxies, and the other is a very narrow maximum at $z \sim z_F$ caused by the luminous epoch of early-type galaxies. The extended redshift distribution with luminosity evolution results in an excess of galaxy count as shown in Figure 8.

The double-peaked feature in the redshift distribution is prominent only in the range of $B_J \sim 21$–$24$ mag.[7] At much brighter magnitudes the second maximum does not appear, and at much fainter magnitudes the two maxima coalesce into a single hump. The double-peaked feature may become unclear if there is a dispersion in $z_F$ (Tinsley 1977). Therefore, once a value of $q_0$ is determined by the $m - z$ relation and the galaxy count, a realistic spread in $z_F$ is evaluated by the redshift distribution.

[7] The second maximum expected in case of the Bruzual $\mu_B = 0.3$ and c models does not show up in Fig. 8 of Bruzual and Kron (1984). This is because very large value of $z_F (\sim 50)$ is assumed implicitly in their paper.

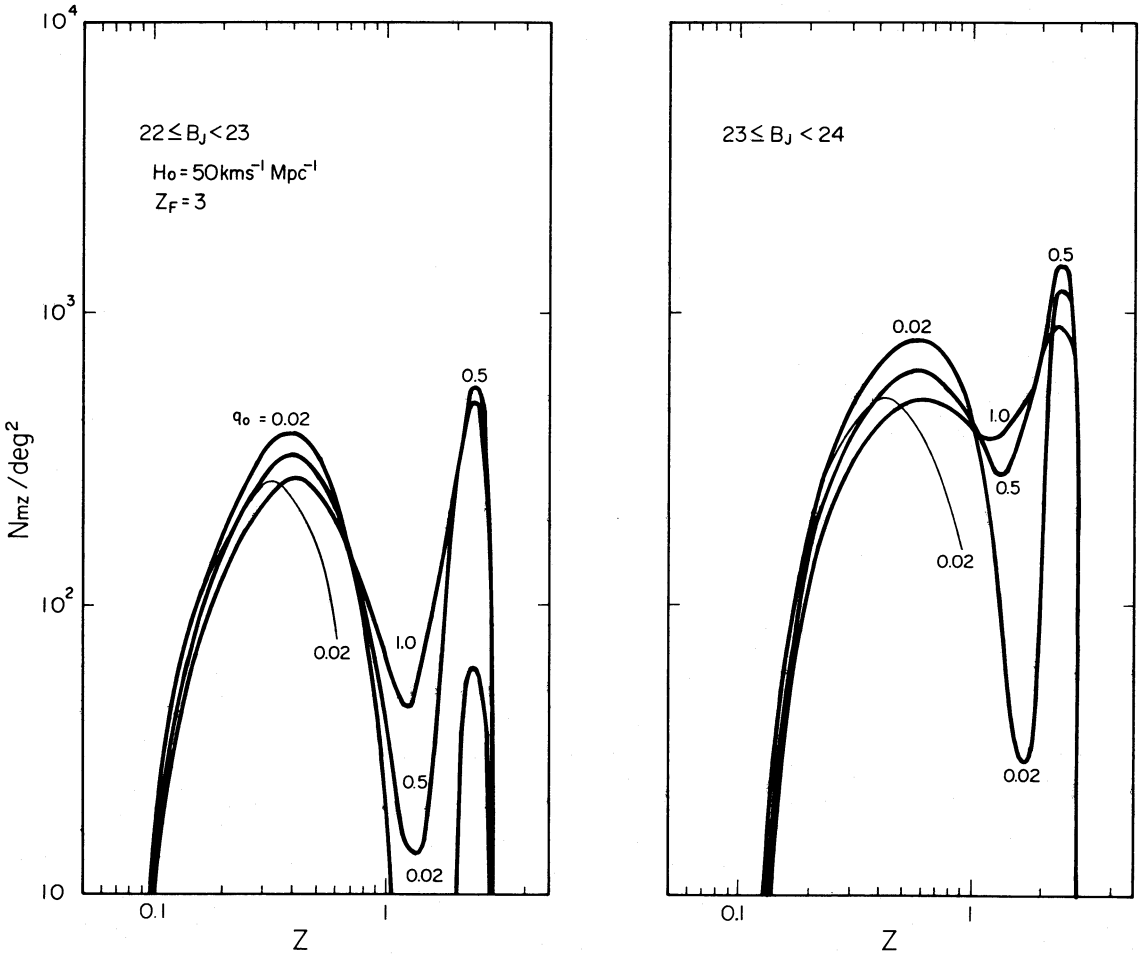


FIG. 11.—Frequency distribution of galaxies in a unit area of 1 deg$^2$ binned into a logarithmic interval of redshift $\Delta \log z = 0.07$ for two magnitude ranges of $B_J = 22$–$23$ mag and 23–24 mag. Thick and thin lines represent the models for evolving and nonevolving galaxies, respectively. Number beside each line is the value of $q_0$ provided $z_F = 3$.

## V. EXTRAGALACTIC BACKGROUND LIGHT

The intensity of the extragalactic background light (EBL) at wavelength $\lambda$ per steradians is given by

$$I_\lambda = \frac{c}{4\pi H_0} \sum_{i=1}^{5} \mathscr{L}_{0\lambda} A^i(\lambda) , \tag{16}$$

with the accumulation factor (Jakobsen 1980)

$$A^i(\lambda) = \int_0^{z_F} \frac{f^i_{\lambda/(1+z)}(z)/f^i_\lambda(0)}{(1+z)^4(1+2q_0 z)^{1/2}} dz , \tag{17}$$

where the suffix $i$ indicates the quantity of galaxy type $i$. The normalization to the EBL defined as $I_{0\lambda} = (c\mathscr{L}_{0\lambda})/(4\pi H_0)$ at $\lambda \sim 0.46$ $\mu$m is tabulated in Table 2 (the summation over $i$ is abbreviated here).

Figure 12 shows the EBL calculated in the wavelength range of $\lambda = 0.36$–$3.4$ $\mu$m. The thick and thin lines represent the evolution and no evolution models, respectively. The EBL without evolution mainly depends on $q_0$, while on both $q_0$ and $z_F$ with evolution. The numbers besides the lines indicate the values of the parameters. The evolution enhances $I_\lambda$ by a factor of 2 or 3, but it does not change the shape of the spectrum appreciably.

The intensity defined in equation (16) is equivalent to

$$I_\lambda = I_{A0\lambda} \int_{-\infty}^{+\infty} \mathrm{dex}\,(-0.4m_\lambda) n(m_\lambda) dm_\lambda , \tag{18}$$

provided $\omega = 1$ in $n(m_\lambda)$, where $I_{A0\lambda}$ is the absolute intensity of the zeroth-magnitude A0 star. It is evident from the form of the integrand in equation (18) that galaxies contribute most to the EBL at some intermediate magnitude between bright and faint magnitude limits, i.e., $B_J \sim 20$ mag, for example (Tinsley 1977). Smaller $q_0$ enhances the EBL owing to larger $n(m_\lambda)$ at such intermediate magnitude (see Figs. 8–10). On the other hand, the EBL is insensitive to $z_F$ because a change of $z_F$ merely changes the number of very faint galaxies. Taking a case of $(H_0, q_0, z_F) = (50\ \mathrm{km\ s^{-1}\ Mpc^{-1}}, 0.02, 3)$, we show in Figure 13 the contribution of each galaxy type to the EBL. In both cases with and without evolution, E/S0 galaxies dominate the EBL at $\lambda > 1$ $\mu$m, while Sabc galaxies do so at $\lambda < 0.7$ $\mu$m. The evolution brightens E/S0 considerably in the past, but it dims Scdm. As a result, E/S0 and Scdm contribute equally to the EBL at $\lambda < 0.7$ $\mu$m.

The observed upper limit on $I_\lambda$ at $\lambda = 0.51$ $\mu$m by Dube, Wickes, and Wilkinson (1977) is much higher than the predicted values of the evolution models. Recently the infrared EBL was observed by Matsumoto, Akiba, and Murakami (1987) using data of the rocket experiment. Fairly large energy fluxes are observed in the $K$ and $L$ bands as well as in several narrow bands, but only the upper limits are obtained in the $J$ and $M$ bands. The detected intensities exceed our result by an order of magnitude even if luminosity evolution is taken into account.

The theoretical EBL was first considered by Partridge and Peebles (1967) at $\lambda \sim 0.1$–$100$ $\mu$m, using their own models of galactic evolution. They calculated the EBL in two extreme ways assuming no luminosity evolution of galaxies (model 1) and assuming that massive pregalactic stars produce the primordial helium ($\sim$20% by mass) and bring about the hyperluminous epoch prior to formation of galaxies (model 4). (Afterward, Tinsley 1973 studied the effect of galactic evolution on the resulting EBL at $\lambda \sim 0.1$–$10$ $\mu$m extensively and

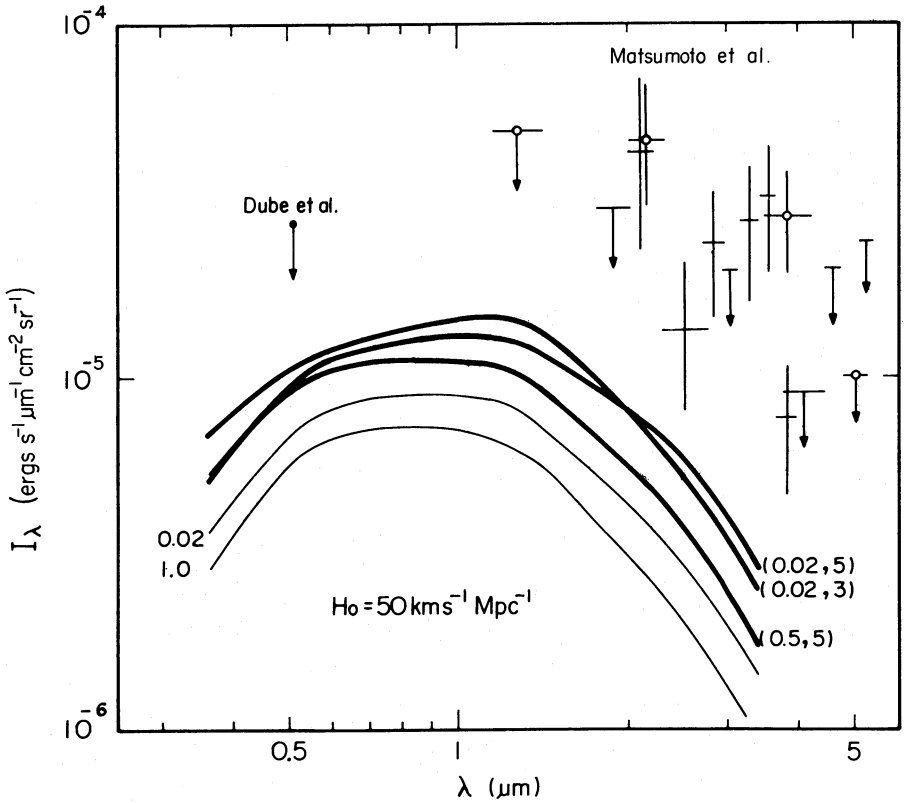


FIG. 12.—Intensity of extragalactic background light as a function of wavelength $\lambda$. Thick and thin lines represent the models for evolving and nonevolving galaxies, respectively. Number beside each thin line is the value of $q_0$, and numbers in parentheses beside each thick line are the values of $q_0$ and $z_F$.

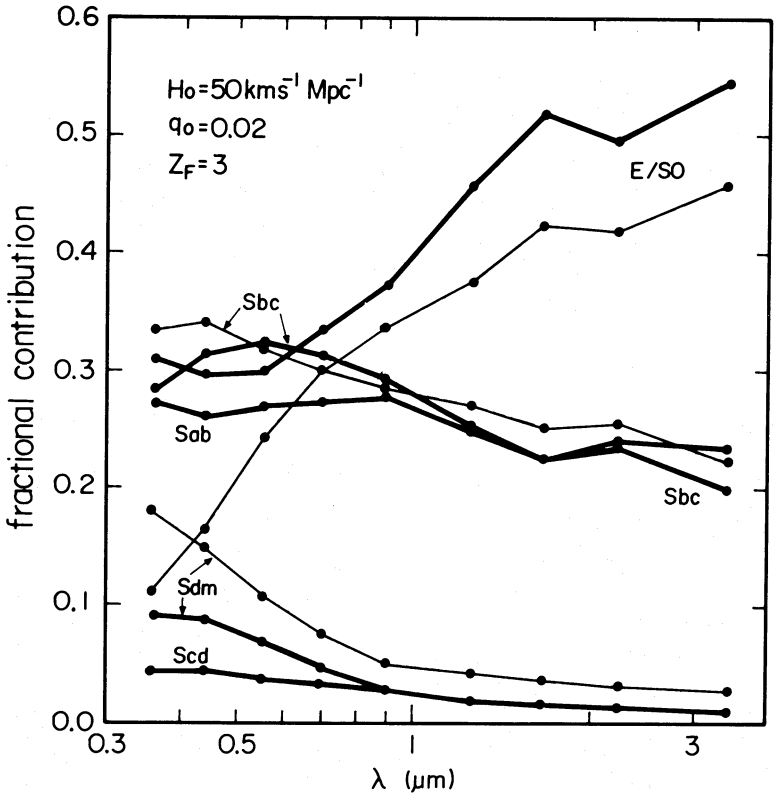


FIG. 13.—Fractional contribution of each galaxy type to the EBL as a function of wavelength $\lambda$ for the case of $(H_0, q_0, z_F) = (50 \text{ km s}^{-1} \text{ Mpc}^{-1}, 0.02, 3)$. Thick and thin lines represent the evolving and nonevolving galaxies, respectively. Note that the contributions of nonevolving Sab and Scd are not shown.

Bruzual 1981 and Wyse 1986 investigated a similar problem at $\lambda \sim 0.1$–$0.6$ $\mu$m. All their EBLs predict the intensities between the models 1 and 4 of Partridge and Peebles 1967.) Especially the model 1 predicts the intensities $\sim 2$ times larger than our result. At present it is known that the normalization $I_{0\lambda} = 4.30 \times 10^{-5}$ ergs s$^{-1}$ $\mu$m$^{-1}$ cm$^{-2}$ sr$^{-1}$ at $\lambda \sim 0.43$ $\mu$m adopted by Partridge and Peebles (1967) leads to an appreciable excess in the galaxy number count systematically at bright magnitudes (e.g., Ellis 1983). Therefore, constrained strictly by the galaxy count over the range of $B_J = 12$–$16$ mag, the smaller normalization $I_{0\lambda} = 2.52 \times 10^{-5}$ ergs s$^{-1}$ $\mu$m$^{-1}$ cm$^{-2}$ sr$^{-1}$ at $\lambda \sim 0.46$ $\mu$m is appropriate as in our analysis. After reducing the normalization by this amount, even the model 4 which gives the brightest EBL predicts the intensities below the detected values in the infrared region. Therefore, some other energy sources should be required if we take the observations at face value and if it is of extragalactic origin. Alternatively, it may be due to other origins than extragalactic background.

## VI. SUMMARY

In this paper we calculated various cosmological relations for several values of the cosmological deceleration parameter $q_0$ and the formation redshift of galaxies $z_F$. The effect of luminosity evolution of galaxies was incorporated using Arimoto and Yoshii (1986, 1987) models. The relations examined here are the magnitude-redshift relation, the color-redshift relation, the differential number count, the redshift distribution of a magnitude-limited sample of galaxies, and the extragalactic background light. The results are summarized below.

### *a) The Apparent Magnitude versus Redshift Relation for Giant Elliptical Galaxies*

The apparent magnitude at a given $z$ becomes brighter for larger $q_0$ or smaller $z_F$. The galactic evolution shifts the magnitude brightward significantly and brings about a turnup of magnitude which is insensitive to redshift at $z > 1$. The observed $V$ magnitudes of giant ellipticals have almost constant values of $V \sim 22$–$23$ mag at $0.4 < z < 1.8$, which favors the value of $q_0$ far exceeding unity in case without galactic evolution. Otherwise, the galactic evolution reduces it to $q_0 \sim 0.5$–$1.0$ provided $z_F \sim 3$–$5$. The model for $q_0 = 0.02$ predicts a value of $V$ which is $\sim 2$ mag fainter than the observed ones at $z \sim 1$ even if the evolutionary brightening is taken into account. Therefore, low value of $q_0$ is unfavorable, and the $V - z$ relation suggests larger value of $q_0$.

The trends of the $K - z$ relation with $q_0$, $z_F$, and galactic evolution are similar to those of the $V - z$ relation. At present, the scatter in observational data reduces an advantage in the infrared passband where our analysis is not affected by uncertain ultraviolet SEDs.

### *b) The Color versus Redshift Relation for Giant Elliptical Galaxies*

The color-redshift relation does not depend on either $q_0$ or $z_F$ in the no evolution model. The galactic evolution shifts the color blueward; the shift becomes larger for larger $q_0$ or smaller $z_F$. The fact that the observed $B-V$ and $V-R$ colors are bluer than the relation without evolution suggests that

ellipticals underwent spectral evolution and hence luminosity evolution in the past. However, reliable determination of $q_0$ and $z_F$ is not possible owing to the scatter in the data and underestimate of our $E$ correction at $z > 0.2$ for $B-V$ and at $z > 0.5$ for $V-R$. The infrared $H-K$ colors with galactic evolution show a relatively weak dependence on $z$ up to $z \sim 1$. The large scatter in the data $\sim$0.5–1 mag at $z > 0.5$ obscures difference between the galactic evolution and the cosmological model.

### c) *The Differential Number Count of Galaxies*

The count increases from bright magnitudes as $d \log n(m)/dm = 0.6$ because bright galaxies are assumed to be distributed homogeneously in space. As apparent magnitude increases, the count increases less rapidly due to the effect of the $K$ dimming, reach a maximum, and then decreases monotonically. The total number of galaxies becomes smaller for larger $q_0$ or smaller $z_F$. The magnitude at which the count begins to decline is sensitive to the galactic evolution. Given $q_0$ and $z_F$, the evolutionary brightening of early-type galaxies shifts the magnitude brightward without changing the peak count appreciably. Since the observed count $\log n(m) \sim 4.3$–4.6 at $B_J \sim 25$ mag already exceeds the peak count for $q_0 = 1.0$, high value of $q_0$ is unfavorable. However, the peak counts for $q_0 = 0.02$ and 0.5 are reconcilable to the observed count at $B_J \sim 25$ mag if evolutionary brightening is taken into account.

The trends of the model $R_F$ and $K$ counts with $q_0$, $z_F$, and galactic evolution are similar to those of the model $B_J$ count. At present we have not obtained data of good quality yet. Future observations are expected to make practical application of the model counts in these passbands.

### d) *The Redshift Distribution for a Magnitude-limited Sample of Galaxies*

The redshift distribution for nonevolving galaxies has a single maximum and falls off sharply toward higher redshift, while the distribution for evolving galaxies has two maxima on either sides of the break; a broad maximum for low-redshift galaxies and a sharp maximum near $z_F$. This double-peaked feature in the redshift distribution is prominent only in the range of $B_J \sim 21$–24 mag where the effects of $q_0$ and galactic evolution do not show up in the number count yet. Therefore, the redshift distribution will provide a powerful test for constraining the cosmological model.

### e) *The Extragalactic Background Light*

The EBL intensity without galactic evolution mainly depends on $q_0$, while on both $q_0$ and $z_F$ with evolution. The EBL is enhanced for smaller $q_0$, but is insensitive to $z_F$ because a change of $z_F$ merely changes the number of very faint galaxies which contribute negligibly to the EBL. The galactic evolution enhances the EBL by a factor of 2 or 3 without changing the shape of the spectrum appreciably.

The detected EBL intensities in the near-infrared region by Matsumoto, Akiba, and Murakami (1987) are much higher than the predicted values even if the galactic evolution is taken into account. Therefore, some other energy sources should be required if we take the observations at face value and if it is of extragalactic origin.

Summarizing above, the magnitude-redshift relation favors high $q_0$ models, while the galaxy number count favors low $q_0$ models. At present we do not settle the deceleration parameter definitely, but the value of $q_0 \sim 0.5$ provided $z_F \sim 3$–5 seems to be consistent with the available observations if we take into account the effect of luminosity evolution of galaxies. We hope that further observations of good quality will probe more accurately the cosmological parameters and galactic evolution.

We thank T. Matsumoto for providing the observational data prior to publication and useful discussion. We also thank an anonymous referee for comments. This work was supported in part by Scientific Research Funds of Ministry of Education, Science, and Culture of Japan (No. 60740129).

## REFERENCES


Aaronson, M. 1978, *Ap. J. (Letters)*, **221**, L103.
Aaronson, M., Cohen, J. G., and Mould, J. 1978, *Ap. J.*, **223**, 824.
Allen, A. J. 1973, *Astrophysical Quantities* (London: Athlone).
Arimoto, N., and Yoshii, Y. 1986, *Astr. Ap.*, **164**, 260.
———. 1987, *Astr. Ap.*, **173**, 23.
Bertola, F., Capaccioli, M., and Oke, J. B. 1982, *Ap. J.*, **254**, 494.
Bruzual, A. G. 1981, *Rev. Mexicana Astr. Ap.*, **6**, 19.
———. 1983*a*, *Ap. J.*, **273**, 105.
———. 1983*b*, *Rev. Mexicana Astr. Ap.*, **8**, 63.
Bruzual, A. G., and Kron, R. G. 1980, *Ap. J.*, **241**, 25.
Bruzual, A. G., and Spinrad, H. 1981, in *The Universe at Ultraviolet Wavelength*, ed. R. D. Chapman (Greenbelt: NASA/Goddard Space Flight Center), p. 731.
Code, A. D., and Welch, G. A. 1979, *Ap. J.*, **228**, 95.
Code, A. G., Welch, G. A., and Page, T. L. 1972, in *The Scientific Results from the Orbiting Astronomical Observatory*, ed. A. D. Code (Washington, DC: NASA SP-310), p. 559.
Coleman, G. D., Wu, C.-C., and Weedman, D. W. 1980, *Ap. J. Suppl.*, **43**, 393.
Couch, W. J., and Newell, E. B. 1984, *Ap. J. Suppl.*, **56**, 143.
Demarque, P., and McClure, R. D. 1977, in *The Evolution of Galaxies and Stellar Populations*, ed. B. M. Tinsley and R. B. Larson (New Haven: Yale University Observatory), p. 199.
de Vaucouleurs, G. 1963, *Ap. J. Suppl.*, **8**, 3.
Djorgovski, S., and Spinrad, H. 1987, *Ap. J.*, in press.
Dube, R. R., Wickes, W. C., and Wilkinson, D. T. 1977, *Ap. J.*, **215**, 51.
Ellis, R. S. 1980, in *Two-Dimensional Photometry*, ed. P. Crane and K. Kjar (Garching: ESO), p. 339.
———. 1983, in *The Origin and Evolution of Galaxies*, ed. B. J. T. Jones and J. E. Jones (Dordrecht: Reidel), p. 255.
Felton, J. E. 1977, *A.J.*, **82**, 861.
Frogel, J. A., Persson, S. E., Aaronson, M., and Matthews, K. 1978, *Ap. J.*, **220**, 75.
Grasdalen, G. L. 1980, in *IAU Symposium 92, Objects of High Redshift*, ed. G. Abell and P. J. E. Peebles (Dordrecht: Reidel), p. 269.
Hall, P., and Mackay, C. D. 1984, *M.N.R.A.S.*, **210**, 979.
Hamilton, D. 1985, *Ap. J.*, **297**, 371.
Jakobsen, P. 1980, *Astr. Ap.*, **81**, 66.
Jarvis, J. E., and Tyson, J. A. 1981, *A.J.*, **86**, 476.
Johnson, H. J. 1966, *Ap. J.*, **143**, 189.
King, C. R., and Ellis, R. S. 1985, *Ap. J.*, **288**, 456.
Kirschner, R. P., Oemler, A., and Schechter, P. L. 1978, *A.J.*, **83**, 1549.
———. 1979, *A.J.*, **84**, 951.
Kristian, J., Sandage, A., and Westphal, J. A. 1978, *Ap. J.*, **221**, 383.
Kron, R. G. 1980, *Ap. J. Suppl.*, **43**, 305.
Larson, R. B., and Tinsley, B. M. 1974, *Ap. J.*, **192**, 293.
Lebofsky, M. J. 1981, *Ap. J. (Letters)*, **245**, L59.
Lebofsky, M. J., and Eisenhardt, P. R. M. 1986, *Ap. J.*, **300**, 151.
Lilly, S. J., and Longair, M. S. 1984, *M.N.R.A.S.*, **211**, 833.
Matsumoto, T., Akiba, M., and Murakami, H. 1987, *Ap. J.*, submitted.
Oke, J. B., Bertola, F., and Capaccioli, M. 1981, *Ap. J.*, **243**, 453.
Oke, J. B., and Sandage, A. 1968, *Ap. J.*, **154**, 21.
Partridge, R. B., and Peebles, P. J. E. 1967, *Ap. J.*, **148**, 377.
Pence, W. 1976, *Ap. J.*, **203**, 39.
Peterson, B. A., Ellis, R. S., Kibblewhite, E. J., Bridgeland, M. T., Hooley, T., and Horne, D. 1979, *Ap. J. (Letters)*, **233**, L109.
Sandage, A. 1961, *Ap. J.*, **133**, 355.
———. 1972*a*, *Ap. J.*, **173**, 485.
———. 1972*b*, *Ap. J.*, **178**, 1.
———. 1973, *Ap. J.*, **183**, 711.
Sandage, A., Binggeli, B., and Tammann, G. A. 1985, *A.J.*, **90**, 1759.
Sandage, A., Kristian, J., and Westphal, J. A. 1976, *Ap. J.*, **205**, 688.
Schechter, P. 1976, *Ap. J.*, **203**, 297.
Shanks, T., Stevenson, P. R. F., Fong, R., and MacGillivray, H. T. 1984, *M.N.R.A.S.*, **206**, 767.

Spinrad, H. 1980, in *IAU Symposium 92, Objects of High Redshift*, ed. G. Abell and P. J. E. Peebles (Dordrecht: Reidel), p. 39.
———. 1986, *Pub. A.S.P.*, **98**, 269.
Tammann, G. A., Yahil, A., and Sandage, A. 1980, *Ap. J.*, **234**, 775.
Tinsley, B. M. 1968, *Ap. J.*, **151**, 547.
———. 1972, *Astr. Ap.*, **20**, 383.
———. 1973, *Astr. Ap.*, **24**, 89.
———. 1977, *Ap. J.*, **211**, 621; **216**, 349.
Tinsley, B. M. 1978*a*, *Ap. J.*, **220**, 816.
———. 1978*b*, *Ap. J.*, **222**, 14.
———. 1980, *Ap. J.*, **241**, 41.
Tinsley, B. M., and Gunn, J. E. 1976, *Ap. J.*, **203**, 52.
Weinberg, S. 1972, *Gravitation and Cosmology* (New York: Wiley).
Wells, D. S. 1972, *Univ. Texas Pub.*, No. 13.
Whitford, A. E. 1977, *Ap. J.*, **211**, 527.
Wyse, R. F. G. 1986, *Ap. J.*, **299**, 593.

FUMIO TAKAHARA: Tokyo Astronomical Observatory, University of Tokyo, Mitaka, Tokyo 181, Japan

YUZURU YOSHII: Mount Stromlo and Siding Spring Observatories, Private Bag, Woden P.O., ACT 2606, Australia